Departament de Teoria
del Senyal i Comunicacions
UNIVERSITAT POLITÈCNICA DE CATALUNYA

MULTIDIMENSIONAL SPECKLE NOISE, MODELLING AND FILTERING RELATED TO SAR DATA

by

Carlos López Martínez

Xavier Fàbregas Cànovas, Thesis Advisor

Ph.D. Dissertation

Thesis Committee: Antoni Broquetas i Ibars
Ignasi Corbella i Sanahuja
Jong-Sen Lee
Eric Pottier
Juan Manuel López Sánchez

Barcelona, June 2, 2003

Chapter 7

Multidimensional Speckle Noise Reduction

7.1 Introduction

This chapter addresses the problem of speckle noise reduction in multidimensional SAR imagery on the basis of the noise model presented in Chapter 5 and the WCCE algorithm presented in Chapter 6, with special emphasis to PolSAR data. As it has been demonstrated in Chapter 5, speckle consists in two noise components over the Hermitian product real and imaginary parts of a pair of SAR images, Eq. (5.95). The first noise component has a multiplicative behavior. The second noise component is characterized by an additive behavior, whose variance depends on the coherence between the pair of SAR images, in such a way that the larger the coherence, the lower the variance. Both terms do not depend, directly, on the Hermitian product average phase difference. But, as it has been proved, this phase has an important impact on the final speckle noise nature for the Hermitian product real and imaginary parts, since it introduces a modulation in the multiplicative speckle noise term. The availability of the speckle noise model for the Hermitian product has been employed as the basis to define a vectorial speckle noise model for multidimensional SAR imagery under the covariance matrix formulation, Eq. (5.106).

From the results derived in Chapter 5, it is clear that the speckle noise nature, in the case of multidimensional SAR imagery, depends on the correlation structure between the different SAR images. The main consequence of this result, as it will be demonstrated, is that, optimum speckle reduction has to be performed according to this correlation structure. Chapter 6 addressed the complex correlation estimation problem, in the field of InSAR imagery, on the basis of the wavelet analysis theory and on the interferometric phasor noise model derived in Chapter 4. As it has been proved in Section 5.2 at Chapter 5, the interferometric phasor noise model can be extended to multidimensional SAR imagery. Thus, the algorithm introduced in Chapter 6 will be employed next to estimate the multidimensional SAR imagery correlation structure, as a first step to reduce multidimensional speckle noise. Hence, all the series of ideas presented in the previous chapters are employed in the following as the basis for the multidimensional speckle noise reduction problem.

The next section of this chapter gives an overview concerning the state of the art on multidimensional speckle noise reduction. As it will be shown, the lack of a multidimensional speckle noise model has represented a limitation concerning the definition of an optimal speckle noise reduction algorithm. The second part of the chapter is devoted to prove that the algorithm presented in the previous chapter can be extended to estimate the complex correlation coefficient between two correlated SAR images, and by extension the multidimensional SAR imagery correlation structure. This extension comes to confirm the theory presented in Chapter 5, in which the multidimensional speckle noise model was derived on the basis of the phase difference phasor noise model. As noticed throughout the previous chapter, this

new algorithm presents some important features as the spatial resolution maintenance and the ability to estimate coherence information completely independent from the phase information. These issues make the algorithm suitable to estimate the multidimensional SAR imagery correlation structure.

The last part of this chapter presents several alternatives to reduce multidimensional speckle noise effects, with special emphasis to PolSAR data. An important aspect which will be discussed is the way the covariance matrix elements can be processed. It will be demonstrated that its elements can be processed differently without skewing or damaging polarimetric information, under the assumption that they are processed according to the multidimensional speckle noise model presented in Chapter 5.

7.2 State of the Art

The speckle noise problem in multidimensional SAR imagery has been addressed, quite often, from the point of view of PolSAR data, as it can be concluded from literature. This is due to the fact that PolSAR presents a big potential in order to retrieve relevant information about the scattering process, but also, on the availability of this type of data from existing PolSAR sensors, mainly placed on airborne platforms.

The concept of PolSAR data filtering can be understood as the extraction of a *true* signal corrupted by systems effects and/or noise effects [7]. Additionally, this extraction has to face two fundamental issues. On the one hand, the estimation of the statistical information of distributed scatterers, and, on the other hand, the estimation of morphological information contained in the signal itself. That is, to retrieve the information concerning the shapes and the boundaries of distributed scatterers but also, the information of deterministic scatterers. These two issues are somehow contradictory as shown in the previous chapters, since the larger the statistical information estimation accuracy, the larger the loss on signal morphology information. Depending on which PolSAR data feature wants to be addressed, several types of PolSAR data filtering techniques emerge.

PolSAR data can be understood as a way of diversity, since from a given scatterer, several information channels are available. Therefore, a first type of PolSAR data filtering approaches make use of this way of diversity to reduce noise effects. The result of these techniques is a single intensity image obtained as a combination of the intensities of the different data channels . An incoherent addition of intensities is not optimal, considering noise reduction, as a result of the existing correlation between images. Therefore, in order to maximize noise reduction, decorrelation or whitening techniques are employed [37]. The resulting intensity image maintains the spatial resolution of the original intensities, but the polarimetric information contained in the SAR images correlation structure is lost. A multilook polarimetric whitening filter has been also described [209].

A second group of approaches extend the ideas behind [37] in order to retrieve a set of speckle reduced images. In [39], the authors present an algorithm to derive the speckle reduced images corresponding to the covariance matrix diagonal elements, that is $|S_{hh}|^2$, $|S_{hv}|^2$ and $|S_{vv}|^2$ for PolSAR data expressed in the linear polarization basis $\{\widehat{\mathbf{h}}, \widehat{\mathbf{v}}\}$. In addition, the authors study the possibility to include frequency diversity. Since noise can be supposed to be uncorrelated between non-overlapped frequency bands, PolSAR data at different frequency bands can be employed to increase the number of independent observables in order to maximize noise reduction. In [40], S. Goze and A. Lopes generalized the approach presented in [39] by including all the covariance matrix elements. Additionally, in [209], several filters accounting also for textural information have been presented. Despite these filters are able to provide a set of noise reduced images, polarimetric information is not preserved. In all these cases, filtered images are derived from a combination of the input channels. Therefore, the correlation properties between the different images channels are altered [1]. It has been demonstrated that the correlation structure between the different SAR channels, i.e., the information contained on the covariance matrix, incorporates important information concerning the scatterer's properties. Therefore, the correlation information between SAR images has to be maintained.

The next group of techniques addresses the two issues concerning PolSAR data filtering mentioned above. On the one hand, these techniques try to maintain the signal morphology, but, on the other hand, they also maintain the statistical information concerning the data correlation structure. As it was shown in Section 2.3 at Chapter 2, distributed scatterers are completely determined by second moments, as for instance, the covariance matrix $[C]$. Consequently, this group of techniques work over second order descriptors trying to retrieve the *true* covariance matrix from corrupted data [41]. The PolSAR data filter presented by J.S. Lee *et al.* in [1] represents an important step towards the optimal PolSAR data filter. In this paper, the authors give the basic principles concerning PolSAR data noise filtering, on the basis of the multiplicative speckle noise model for intensity of the SAR images. These principles are:

- PolSAR data noise must be eliminated from second order statistical descriptors as for instance: the covariance $[C]$, the coherency $[T]$ or the Müeller $[M]$ matrices. Second order descriptors determine completely distributed scatterers under the complex Wishart distribution. The best choice to reduce speckle noise is the covariance matrix, since all its entries correspond to Hermitian products.
- The entries of the covariance matrix have to be independently processed without making use of the data correlation structure in order to avoid crosstalk between them, which would corrupt polarimetric information.
- To preserve polarimetric properties, each covariance matrix entry should be filtered considering the surrounding pixels similarly to multilook processing. All the elements should be filtered by the same amount.
- The morphological information concerning signal features, edge sharpness, deterministic targets, etc... has to be maintained. Consequently, the filter has to adapt to this heterogeneity. The approach presented in [1] performs this process employing the local statistic filter [192] in edge-aligned windows [210].

The PolSAR speckle noise filter given in [1] bases speckle noise reduction on the multiplicative noise model for the SAR images intensity, extending it to all the elements of the covariance matrix, despite the authors affirm that the real and imaginary parts of the off-diagonal covariance matrix entries can not be characterized only by a multiplicative noise behavior. As it has been demonstrated in Chapter 5, the speckle noise for these entries can be characterized by two noise components presenting a multiplicative and an additive nature, respectively. Consequently, it can be affirmed, that the approach presented in [1] is suboptimal concerning noise reduction.

The four principles concerning PolSAR data noise reduction given in [1] have been established under the basis of the suboptimal noise model for the covariance matrix entries. Chapter 5 proves that it is possible to separate the covariance matrix signal into a *noise* term and on an *information* term, despite the correlation between SAR images. Consequently, these principles will be redefined at the end of this chapter taking into consideration these new results, and, allowing to define novel PolSAR data filtering techniques.

Under the complex Wishart distribution assumption for PolSAR data, in [211] the authors have develop the maximum likelihood estimator (MLE) for the mean covariance matrix on the basis of Markov random fields and a simulated annealing stochastic optimization method. This filter relies on the capability of Markov random fields to consider relations between neighbor pixels of the image. The authors demonstrate that this approach is able to retrieve the mean covariance matrix information while maintaining most of the structures in the image. Since this approach is based on the complex Wishart distribution for the covariance matrix, it tends to loose the texture information is textured homogeneous areas.

7.3 Multidimensional Coherence Estimation

The complex correlation coefficient between a pair of correlated SAR images represents a key quantity for multidimensional SAR imagery, and of course, for PolSAR. In Chapter 5, it has been demonstrated that

the final speckle noise nature, for the Hermitian product of a pair of SAR images, is controlled precisely by the complex correlation coefficient. Therefore, the multidimensional speckle noise nature, as given by Eq. (5.106), depends on the correlation structure between the different SAR images. One can conclude, consequently, that in order to filter PolSAR data optimally, it is necessary to adapt to this correlation structure.

Considering PolSAR data in the backscattering case, let $\mathbf{k} = [S_{hh}\ S_{hv}\ S_{vv}]^T$ be the scattering vector defined in the linear polarization basis $\{\widehat{\mathbf{h}}, \widehat{\mathbf{v}}\}$. As observed in Eq. (2.168), a factor $\sqrt{2}$ is introduced within the second term S_{hv} to maintain signal span. Since this factor will not affect the following development, the scattering vector can be defined leaving it out. From the scattering vector $\mathbf{k}$, the covariance matrix is defined as $[C] = E\{\mathbf{k}\mathbf{k}^{*T}\}$, see Eq. (2.174) on Section 2.3.4. This matrix is able to characterize completely distributed scatterers, unlike the scattering matrix $[S]$. Hence, speckle noise has to be reduced from $[C]$, or equally, from any other second order statistics descriptor [41]. The complex covariance matrix can be written as the product of three additional matrices

$$[C] = [P][C_n][P] = \begin{bmatrix} \sqrt{\sigma_{hh}} & 0 & 0 \\ 0 & \sqrt{\sigma_{hv}} & 0 \\ 0 & 0 & \sqrt{\sigma_{vv}} \end{bmatrix} \begin{bmatrix} 1 & \rho_{hhhv} & \rho_{hhvv} \\ \rho^*_{hhhv} & 1 & \rho_{hvvv} \\ \rho^*_{hhvv} & \rho^*_{hvvv} & 1 \end{bmatrix} \begin{bmatrix} \sqrt{\sigma_{hh}} & 0 & 0 \\ 0 & \sqrt{\sigma_{hv}} & 0 \\ 0 & 0 & \sqrt{\sigma_{vv}} \end{bmatrix} \tag{7.1}$$

where $\sigma_{kl} = E\{|S_{kl}|^2\}$ for $k, l \in \{\widehat{\mathbf{h}}, \widehat{\mathbf{v}}\}$ and ρ_{klmn} for $k, l, m, n \in \{\widehat{\mathbf{h}}, \widehat{\mathbf{v}}\}$ indicates the complex correlation coefficient between the pair of SAR images S_{kl} and S_{mn}. The matrix $[P]$ contains the information concerning the power in each SAR image, that is, the radiometric information. On the other hand, the matrix $[C_n]$ incorporates the correlation structure of the scattering vector $\mathbf{k}$, which can be considered as a normalized covariance matrix. As one observes in Eq. (7.1), the diagonal elements of $[C_n]$ are equal to one, since the corresponding diagonal elements of the covariance matrix $[C]$ are composed by the Hermitian product of a SAR image by its complex conjugate. This idea has been already employed in Section 5.4.6 to demonstrate that the speckle noise model for the real and imaginary parts of the Hermitian product of a pair of SAR images turns into a multiplicative model when the SAR image intensity is considered. The off-diagonal entries of $[C_n]$ contain the complex correlation coefficients between the different SAR images in $\mathbf{k}$.

In Chapter 6, a new algorithm to estimate the complex correlation coefficient in the InSAR data case has been presented. This algorithm has its basis on the wavelet analysis theory presented in Chapter 3 and on the interferometric phasor noise model developed in Chapter 4. As proved, the use of the wavelet transform allows to estimate, from the interferometric phasor both, the amplitude $|\rho|$ and the phase ϕ_x of the complex correlation coefficient. The concept of the interferometric phasor has been generalized to the phase difference phasor concept in Section 5.3, in such a way that the argument of a unit amplitude phasor consists in the argument of the Hermitian product of a pair of correlated SAR images. This generalization has made possible to obtain the multidimensional speckle noise model. Consequently, this generalization allows to employ also the WCCE algorithm to estimate the correlation structure of multidimensional SAR imagery, that is, to estimate the normalized covariance matrix $[C_n]$.

7.3.1 Normalized Covariance Matrix Estimation

As shown in Chapter 2, the statistical behavior of the Hermitian product of a pair of SAR images is independent of the type of information contained on it, for instance InSAR data or PolSAR data. Therefore, the Hermitian product phase difference measured by the SAR system ϕ can be decomposed as the addition of a term which contains the useful information, denoted by ϕ_x, and a noise term due to speckle, v [20, 184]. This issue has allowed to generalize the concept of modulated coherence beyond InSAR, to a general Hermitian product of SAR images as presented in Chapter 5. In the case of InSAR data, the phase ϕ_x is a deterministic term containing terrain's topography information. On the contrary, over PolSAR data, the phase ϕ_x is a random variable which is defined as the average of the measured

phase difference ϕ. This average phase contains relevant information which can be related with the scatterer's structure. From a point of view of signal processing, the different nature of the phase ϕ_x for InSAR and PolSAR data introduces subtle differences on the modulated coherence term characteristics in each case.

As presented in Chapter 4, the true interferometric phase difference ϕ_x, for a flat surface, can be modelled as given in Section 4.3.1, since it corresponds to a wrapped phase value in the interval $[-\pi, \pi)$. Therefore, the modulated coherence term can be interpreted as the coherence information, given by N_c, modulated by the topography. The steeper the topography, the higher the frequency where N_c is modulated. In the case of PolSAR data, the phase ϕ_x is not a wrapped phase. Despite this fact, the concept of modulated coherence can still be employed. The only difference is that now, the average phase difference modulates the coherence information given by N_c. Since the average phase difference ϕ_x is not wrapped for PolSAR data, the term N_c will appear mainly concentrated over low frequencies.

As given in Section 6.4 at Chapter 6, the WCCE was defined in such a way that low coherence areas are not processed to avoid the introduction of signal distortions in the estimated interferometric phase. Since in the polarimetric case, the phase ϕ_x does not present fringes and the information concerning N_c is concentrated on low-frequencies, a change is introduced in the WCCE algorithm in order to consider this particularity. The change is introduced in the ***Step*** number 2 of the WCCE algorithm, described in page 165. In this step, the WCCE algorithm selects those wavelet coefficients which contain useful information. The change to introduce is to force the WCCE algorithm to select all the coarse approximation coefficients of the wavelet band a_3 as signal coefficients. This is the case if the DWT is calculated with three scales. Otherwise, if the DWT is calculated with $2^{j'}$ wavelet scales, the wavelet coefficients of the scale $a_{j'}$ have to be considered as signal coefficients.

The coarse coefficients at the wavelet scale $a_{j'}$ are obtained as the convolution of the original signal, the interferometric phase difference phasor in this case, with a low-pass filter. On the other hand, the multilook approach employed to estimate coherence, can be considered as a low-pass filter. As a result, it can be assumed that the coherence information contained in the coefficients at the wavelet scale $a_{j'}$ has the same properties as the coherence calculated with the multilook filter. Therefore, if all the coefficients of the scale $a_{j'}$ are selected, the information contained in these coefficients is included into the recovered signal. Hence, the recovered signal contains the signal mean value contained on the scale $a_{j'}$ plus the information contained on the selected wavelet coefficients from the additional high frequency scales wavelet scales.

The results presented in Chapter 6 showed that the WCCE is able to estimate the average phase difference as well as the coherence information from the interferometric phasor. In the next sections it will be demonstrated that this algorithm, considering the change introduced above, is able to estimate the complex correlation coefficient of a general Hermitian product, and hence, the multidimensional SAR imagery correlation structure. The results will focus on PolSAR data.

7.3.2 Normalized Covariance Matrix Estimation: Real PolSAR Data

This section is focused on presenting results concerning the estimation of the average phase difference ϕ_x and the coherence $|\rho|$ in the case of Hermitian products of pair of SAR images acquired with different combinations of polarizations for transmission and reception. Therefore, at the end of this section, it will be concluded that the WCCE algorithm can estimate the information contained in the normalized covariance matrix $[C_n]$ with high spatial resolution. In order to perform these tests, an E-SAR fully polarimetric dataset acquired over the Oberpfaffenhofen (Germany) test site is employed.

E-SAR PolSAR Data: Oberpfaffenhofen (Germany)

The data employed in this section correspond to a fully polarimetric dataset at L-band (1.3 GHz), acquired in the linear polarization basis $\{\widehat{\mathbf{h}}, \widehat{\mathbf{v}}\}$, with the E-SAR system. The imaged area corresponds to the Oberpfaffenhofen test site. In this case, the phase differences corresponding to the covariance matrix entries $S_{hh}S_{vv}^*$ and $S_{hh}S_{hv}^*$ are analyzed. Fig. 7.1 presents the 1024 by 1024 pixel images of these phase differences.

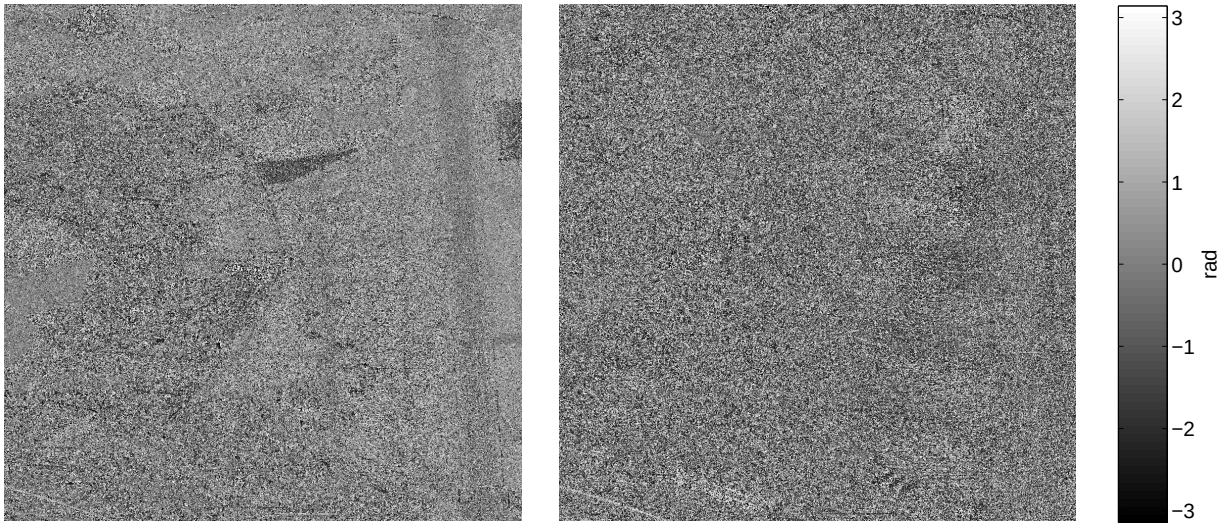

(a) ϕ_{hhvv} (b) ϕ_{hhhv}

Figure 7.1: Hermitian products phase differences. (a) $S_{hh}S_{vv}^*$ phase. (b) $S_{hh}S_{hv}^*$ phase.

As one observes from Fig. 7.1, the phase ϕ_{hhvv} contains less noise than ϕ_{hhhv}. These two phases have been processed with the WCCE algorithm in order to retrieve the complex correlation coefficients of the covariance matrix entries $S_{hh}S_{vv}^*$ and $S_{hh}S_{hv}^*$, denoted by ρ_{hhvv} and ρ_{hhhv} respectively. As in the case of InSAR data, information concerning the actual values of ρ_{hhvv} and ρ_{hhhv} is not available. Consequently, in order to have a quantitative analysis of the derived results, it will be performed by comparing the results of the WCCE algorithm and the results derived with a multilook filter.

The WCCE algorithm is applied with the same parameters as in the InSAR data case. Concerning the threshold, th_w takes a value equal to -1. The next point consists in selecting the wavelet filter to perform the DWPT process. In Chapter 6, some criteria to select the wavelet filter on the basis of interferometric phase noise reduction were given. Since PolSAR and InSAR data are statistically equal, these criteria are exported to the PolSAR data case. Hence, considering this issue, the polarimetric phase differences presented in Fig. 7.1 have been processed with the WCCE algorithm to estimate the complex correlation coefficient. The DWPT is calculated with the Daubechies filters of 10 and 40 coefficients, in order to observe any filter dependent effect. In addition, the complex correlation coefficients have been estimated with the multilook approach by means of a 5 by 5 pixel window.

Fig. 7.2 presents the results concerning the covariance matrix term $S_{hh}S_{vv}^*$, obtained with the multilook filter and the WCCE algorithm. As it follows from these results, no large differences can be noticed between the different estimated quantities. The results derived with the WCCE algorithm contain the same information as the results derived with the multilook approach. Additionally, the results corresponding to the WCCE algorithm, obtained with different wavelet filters, are very similar. This confirms the fact, found for InSAR data, that the filter length, in the case of the Daubechies family of filters, does not play an important role if the length is larger than 10 coefficients. The use of large response filters is advantageous since spatial details are slightly better preserved.

The estimated coherence values with the multilook filter and the WCCE algorithm have been quantitatively compared. To perform this analysis, the difference coherence image $|\widehat{\rho}_{MLT}| - |\widehat{\rho}_{WLT}|$ has been

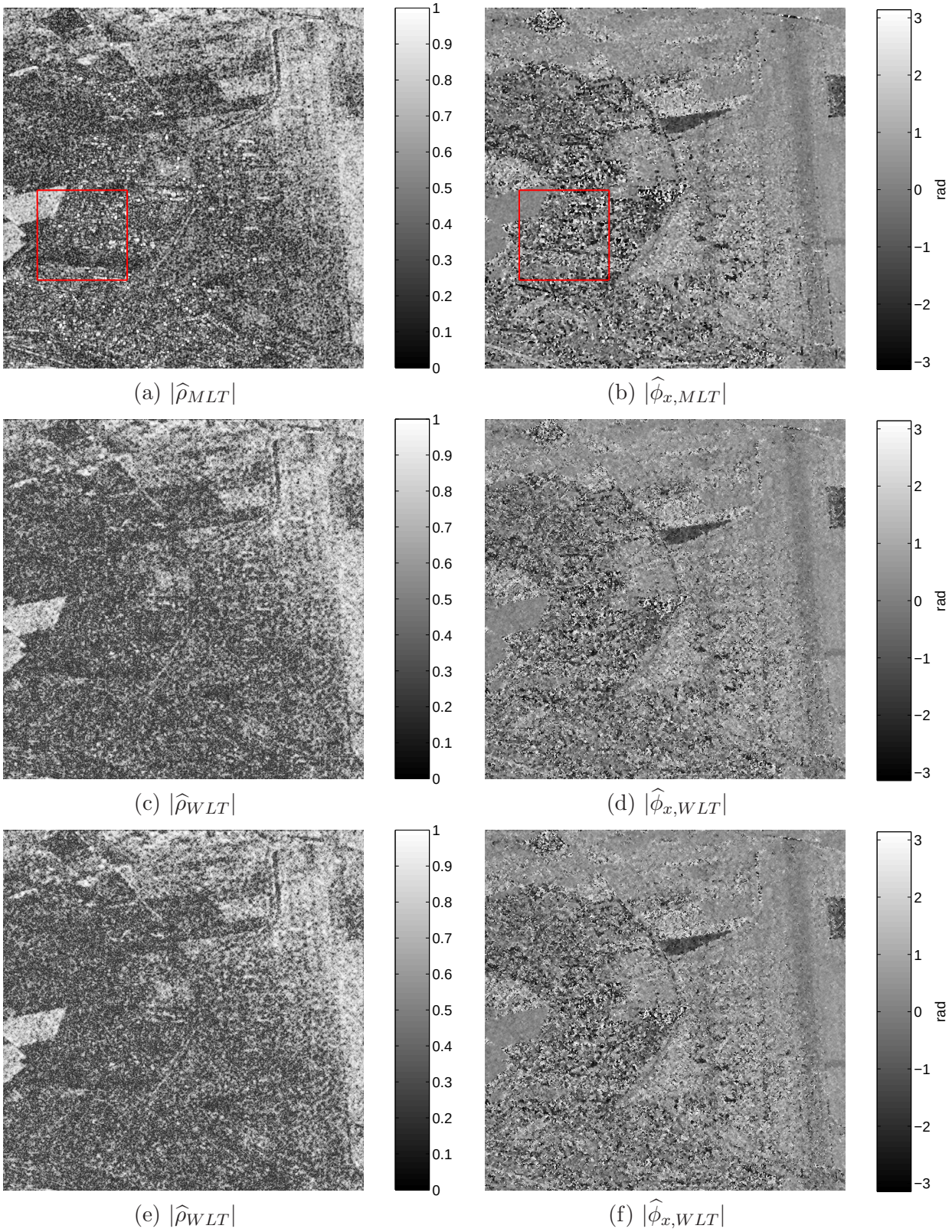

(a) $|\widehat{\rho}_{MLT}|$ (b) $|\widehat{\phi}_{x,MLT}|$

(c) $|\widehat{\rho}_{WLT}|$ (d) $|\widehat{\phi}_{x,WLT}|$

(e) $|\widehat{\rho}_{WLT}|$ (f) $|\widehat{\phi}_{x,WLT}|$

Figure 7.2: Estimated complex correlation coefficient $|\rho| \exp(j\phi_x)$ with the different approaches for the covariance matrix entry $S_{hh}S_{vv}^*$. (a) and (b) Multilook with a 5 by 5 pixel window. (c) and (d) WCCE with 10 coefficient Daubechies filter. (e) and (f) WCCE with 40 coefficient Daubechies filter.

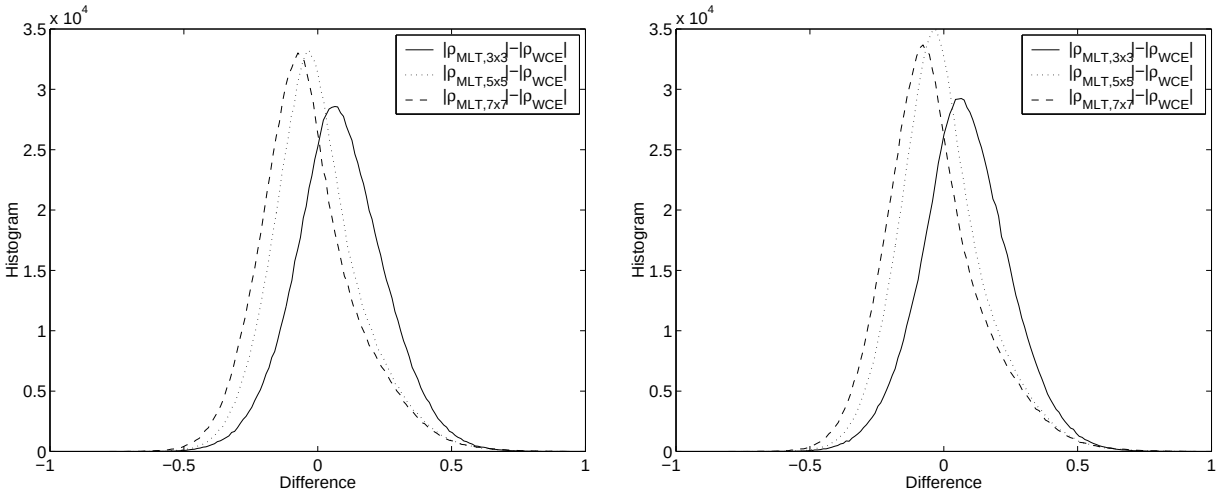

Figure 7.3: Histograms of the difference of the coherence $|\rho_{hhvv}|$ estimated with the WCCE algorithm (with the Daubechies filters of 10 and 40 coefficients) and the Multilook filter for several windows dimensions.

		MLT, 3x3	MLT, 5x5	MLT, 7x7
WCCE Daub. 10	$\mathrm{E}\{\lvert\widehat{\rho}_{MLT}\rvert - \lvert\widehat{\rho}_{WLT}\rvert\}$	0.084	-0.002	-0.037
	$\sigma\{\lvert\widehat{\rho}_{MLT}\rvert - \lvert\widehat{\rho}_{WLT}\rvert\}$	0.169	0.169	0.179
WCCE Daub. 40	$\mathrm{E}\{\lvert\widehat{\rho}_{MLT}\rvert - \lvert\widehat{\rho}_{WLT}\rvert\}$	0.082	-0.004	-0.039
	$\sigma\{\lvert\widehat{\rho}_{MLT}\rvert - \lvert\widehat{\rho}_{WLT}\rvert\}$	0.166	0.167	0.179

Table 7.1: Mean value and standard deviation of the difference between the coherence calculated with a multilook (MLT), as given in the columns, and the WCCE algorithm with the wavelet filter as given in the rows.

calculated with the coherence values estimated with both approaches. In this case, the multilook filter has been applied with 3 by 3, 5 by 5 and 7 by 7 pixel windows, whereas the DWPT in the WCCE algorithm has been calculated with the Daubechies filters of 10 and 40 coefficients. The histograms of the difference coherence images are presented in Fig. 7.3, whereas the mean and standard deviation values of these histograms are given by Table 7.1. One can observe from these results, that the length of the wavelet filter does not play an important role when the coherence value is considered.

The mean values of the difference coherence images, Table 7.1, show that the values obtained with the 3 by 3 pixel multilook present an overestimation of the coherence value, with respect to the estimation given by the WCCE algorithm, larger than an 8% of the maximum coherence value. This bias is the result of the overestimation introduced by the averaging window since, as demonstrated in [113]. It can be observed that for larger multilook window dimensions, the coherence value given by the WCCE algorithm overestimates the coherence value with a bias less than 0.5% of the maximum coherence value, if compared with a 5 by 5 pixel multilook and with a 4% bias in the case of 7 by 7 pixel multilook. It can be concluded, therefore, that the WCCE, with the given parameters, is able to estimate coherence values with the accuracy of a 5 by 5 or 7 by 7 pixel multilook. In this case, the bias is lower than a 5% of the maximum coherence value.

Until now, the performance of the WCCE has been studied from a global point of view. In the following, a local analysis is presented, since as shown in the previous chapter, the use of the wavelet analysis theory allows to obtain an estimation of the complex correlation coefficient with a high spatial accuracy. In Figs. 7.2a and 7.2b, a 256 by 256 pixel area has been marked with a red square, where the spatial properties of the WCCE algorithm are studied in the PolSAR data case. Since long Daubechies filters provide to the WCCE algorithm a slightly better performance in terms of spatial resolution maintenance, the 40 coefficient Daubechies filter is employed to perform this analysis. Fig. 7.4 gives the detailed

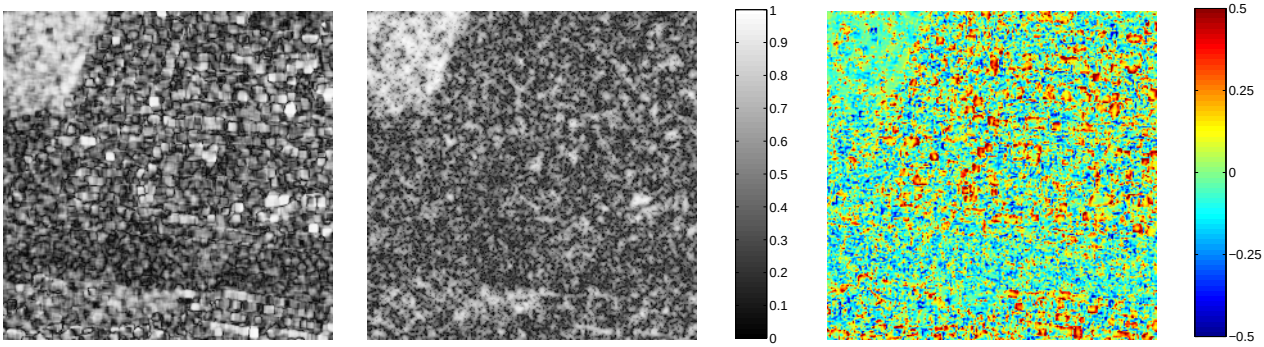

(a) $|\widehat{\rho}_{MLT}|$ (b) $|\widehat{\rho}_{WLT}|$ (c) $|\widehat{\rho}_{MLT}| - |\widehat{\rho}_{WLT}|$

Figure 7.4: 256 by 256 pixel detail image of the term $S_{hh}S_{vv}^{*}$ coherence. (a) Estimated coherence with a 5 by 5 multilook. (b) Estimated coherence with the WCCE algorithm and a 40 coefficient Daubechies filter. (c) Difference image.

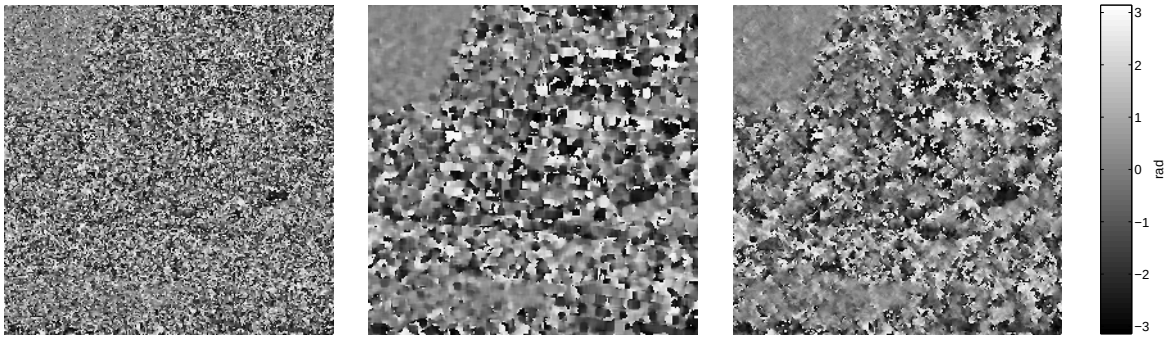

(a) ϕ (b) $\widehat{\phi}_{x,MLT}$ (c) $\widehat{\phi}_{x,WLT}$

Figure 7.5: 256 by 256 pixel detail image of the term $S_{hh}S_{vv}^{*}$ phase difference. (a) Original phase. (b) Estimated phase with a 5 by 5 multilook. (c) Estimated phase with the WCCE algorithm and a 40 coefficient Daubechies filter.

images of the estimated coherence values with a 5 by 5 multilook filter and the WCCE algorithm, with the DWPT obtained with the 40 coefficient Daubechies filter, as well as the difference image. From Figs. 7.4a and 7.4b it is clear that the multilook estimation is affected by the analysis window. This effect does not appear over the value estimated with the WCCE algorithm. Within this area, two homogeneous areas can be noticed. On the one hand, the high coherence area on the upper left-hand corner, and, on the other hand, the low coherence area crossing the lower part of the image. In these cases, both approaches estimate in average the same coherence value. The other areas of the detail images contain point scatterers with high coherence values. The shape of these scatterers is clearly affected by the analysis window. From the difference image, 7.4c, it can be observed that the morphology of these points, in this image, is quite often the same, since they appear as a point with a value close to zero surrounded by a red contour introduced by the window analysis of the multilook filter. Hence, both approaches are able to estimate the right coherence value at the position of the point or deterministic scatterers, but whereas the multilook approach extends its influence to the surroundings, the WCCE maintains the shape.

The performance of the WCCE algorithm to maintain the original spatial resolution and to maintain image details can be also observed in the case of the estimated phase $\widehat{\phi}_x$. Fig. 7.5 presents the results concerning phase estimation for the areas marked in Fig. 7.2b. The result presented by Fig. 7.5b shows clearly that the estimated phase with the multilook approach is affected by the analysis window. As in the previous case, this distortion destroys the shapes of the different details in the phase image.

The results presented above demonstrate the WCCE algorithm's performance to estimate the complex correlation coefficient for a Hermitian product of a pair of complex SAR images with very good properties concerning spatial resolution. The results presented above concern the study of the covariance matrix

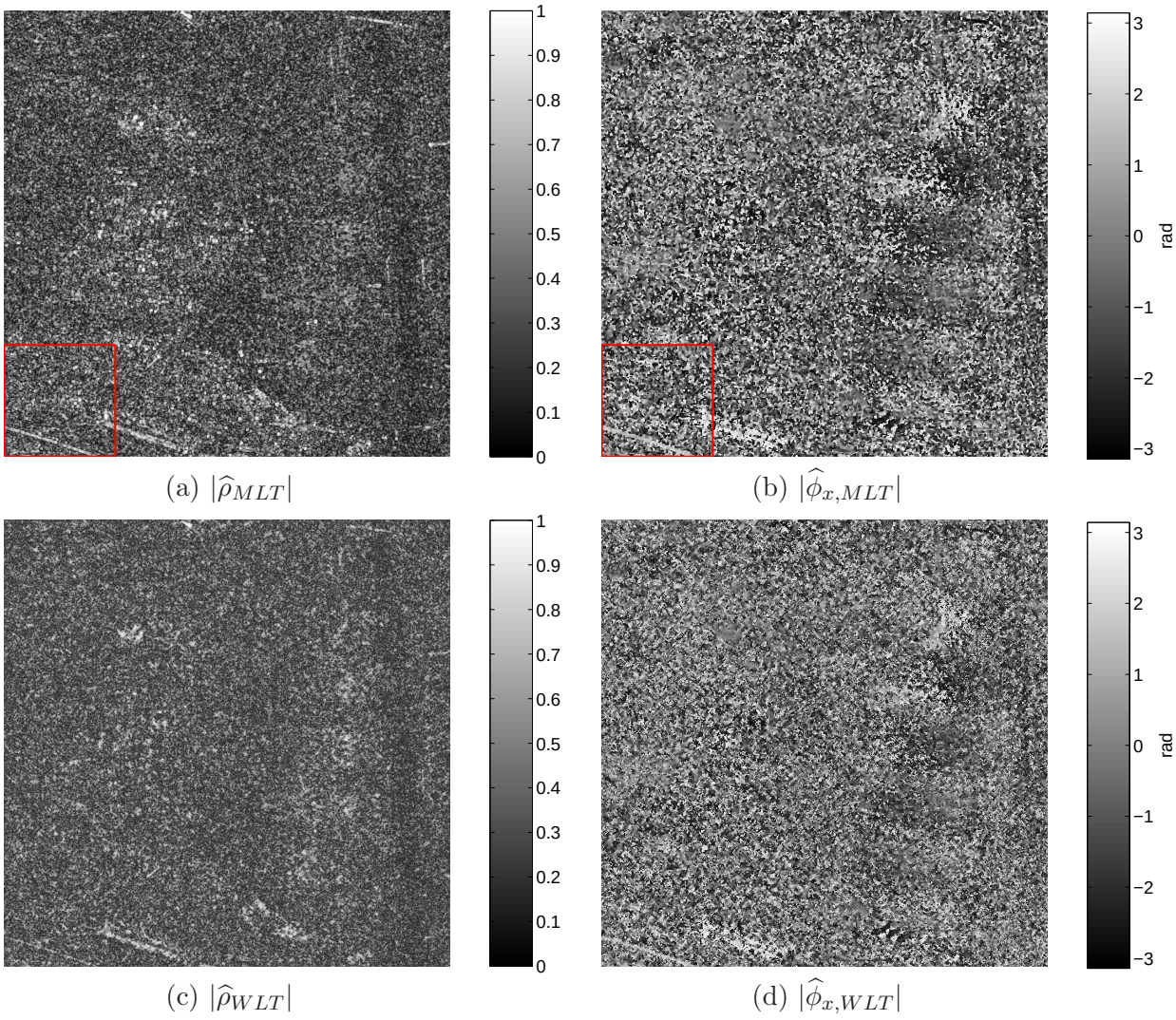

(a) $|\widehat{\rho}_{MLT}|$ (b) $|\widehat{\phi}_{x,MLT}|$

(c) $|\widehat{\rho}_{WLT}|$ (d) $|\widehat{\phi}_{x,WLT}|$

Figure 7.6: Estimated complex correlation coefficient $|\rho|\exp(j\phi_x)$ with the different approaches for the term $S_{hh}S_{hv}^*$. (a) and (b) Multilook with a 5 by 5 pixel window. (c) and (d) WCCE with 10 coefficient Daubechies filter. (e) and (f) WCCE with 40 coefficient Daubechies filter.

entry $S_{hh}S_{vv}^*$. In the following, the term $S_{hh}S_{hv}^*$ is analyzed. From a statistical point of view, both terms are equal. But, since the second entry contains the scattering matrix element S_{hv}, it is characterized by presenting lower coherence values than the term $S_{hh}S_{vv}^*$. The third off-diagonal covariance matrix term $S_{hv}S_{vv}^*$ is also characterized by presenting low coherence values. Therefore, without loss of generality, the covariance matrix $S_{hh}S_{hv}^*$ can be analyzed extending the derived conclusions to the term $S_{hv}S_{vv}^*$. Since the WCCE algorithm only works with phase information, Fig. 7.1b presents the 1024 by 1024 pixel phase image of the covariance matrix entry $S_{hh}S_{hv}^*$. The term $S_{hh}S_{hv}^*$ has been processed with both, the multilook filter applied with a 5 by 5 pixel window and the WCCE algorithm with a $th_w = -1$ and the 40 coefficient Daubechies filter, in order to retrieve the complex correlation coefficient. Fig. 7.6 shows the results derived with both approaches.

Despite the covariance matrix entry $S_{hh}S_{hv}^*$ is characterized by presenting low coherence values as a consequence of the term S_{hv}, no relevant differences can be noticed between the complex correlation coefficient estimated by the multilook and the WCCE approaches. As done before, the covariance values estimated with both approaches are compared. Fig. 7.7 and Table 7.2 contain the results of this comparison for the multilook filter applied with a 3 by 3, a 5 by 5 and a 7 by 7 pixel window and the WCCE approach employing the 40 coefficient Daubechies filter.

Since the covariance matrix entry $S_{hh}S_{hv}^*$ is characterized by lower coherence values than the entry

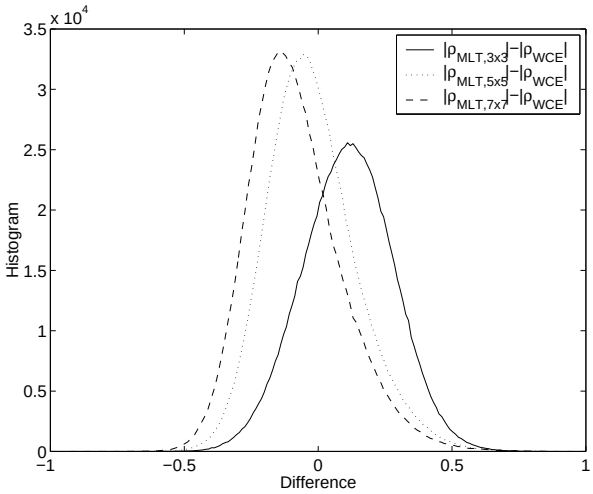

Figure 7.7: Histograms of the difference of the coherence $|\rho_{hhhv}|$, estimated with the WCCE algorithm (with the Daubechies filter of 40 coefficients) and the multilook filter for different windows dimensions.

		MLT, 3x3	MLT, 5x5	MLT, 7x7
Db 40	$\mathrm{E}\{\lvert\widehat{\rho}_{MLT}\rvert - \lvert\widehat{\rho}_{WLT}\rvert\}$	0.110	-0.022	-0.085
	$\sigma\{\lvert\widehat{\rho}_{MLT}\rvert - \lvert\widehat{\rho}_{WLT}\rvert\}$	0.169	0.168	0.174

Table 7.2: Mean difference of the polarimetric coherence $|\rho_{hhhv}|$ estimated with the WCCE algorithm (WLT) and the multilook filer (MLT).

$S_{hh}S_{vv}^*$, the multilook estimated coherence value given in the former case presents a larger bias [113]. In this case, for the multilook applied over a 3 by 3 pixel window the bias is equal to 11% of the maximum coherence value, with respect to the WCCE estimator. The relative difference between the coherence value estimated with the multilook approach and the WCCE algorithm has its minimum for the multilook applied over a 5 by 5 pixel window. Beyond this point, the WCCE coherence value presents an overestimation with respect to the multilook approach. Consequently, considering these results, and those derived in the case of the term $S_{hh}S_{vv}^*$, the WCCE algorithm has a coherence accuracy estimation equal to the one obtained with a 5 by 5 multilook, with the given parameters.

The spatial properties of the processed complex correlation coefficients are analyzed over the areas marked with a red square over Figs. 7.6a and 7.6b. Fig. 7.8 depicts the results concerning coherence estimation. Both estimations show a linear structure with high correlation values crossing the lower left-hand corner of the image. The coherence estimation in this case is a clear example of the effect of the distortion introduced by the averaging window. Whereas the structure is approximately between 5 and 6 pixels wide in the case of the multilook approach, the same structure is only 3 pixels wide in the case of the estimated values with the WCCE algorithm, Fig. 7.8b. If coherences are compared with the amplitude of the complex SAR image S_{hh}, given by Fig. 7.8c, it can be concluded that the estimation obtained with the WCCE algorithm, corresponding to the linear feature, fits better with the structure's shape than the value estimated with the multilook approach. The detail images corresponding to the estimated phase difference are given by Fig. 7.9. As it can be observed, the linear detail appears with more spatial resolution in the case of the value estimated with the WCCE algorithm. As it has been shown in the InSAR data case, the WCCE reduces the maximum quantity of noise, but with the constraint to maintain spatial details and spatial resolution.

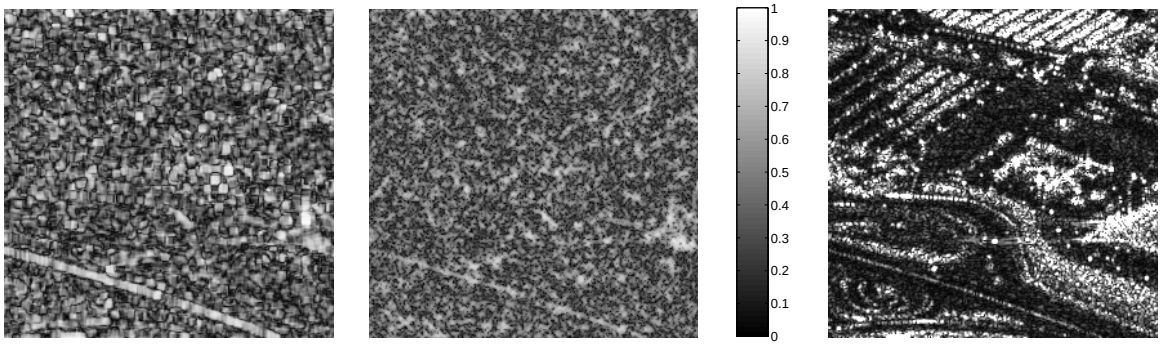

(a) $|\widehat{\rho}_{MLT}|$ (b) $|\widehat{\rho}_{WLT}|$ (c) $|S_{hh}|$

Figure 7.8: 256 by 256 pixel detail image of the term $S_{hh}S_{hv}^{*}$ coherence. (a) Estimated coherence with a 5 by 5 multilook. (b) Estimated coherence with the WCCE algorithm and a 40 coefficient Daubechies filter. (c) Amplitude of the complex SAR image $|S_{hh}|$.

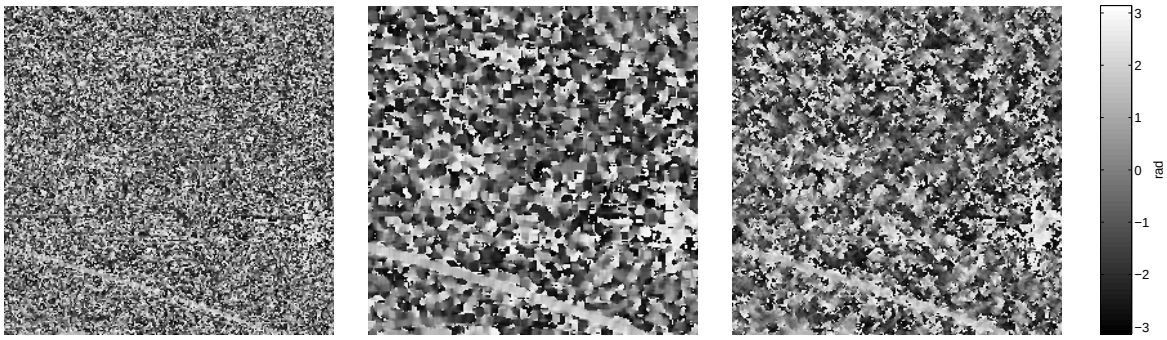

(a) ϕ (b) $\widehat{\phi}_{x,MLT}$ (c) $\widehat{\phi}_{x,WLT}$

Figure 7.9: 256 by 256 pixel detail image of the term $S_{hh}S_{hv}^{*}$ phase difference. (a) Original phase. (b) Estimated phase with a 5 by 5 multilook. (c) Estimated phase with the WCCE algorithm and a 40 coefficient Daubechies filter.

7.3.3 Modulated Coherence Estimation: Concluding Remarks

As it can be concluded from the results presented in this section, the WCCE algorithm is valid to estimate the complex correlation factor ρ between a pair of SAR images for PoLSAR data. As it has been introduced in Section 5.2 at Chapter 5, the scattering vector $\mathbf{k}$ is completely characterized, under the Gaussian scattering assumption, by the covariance matrix $[C]$. Generalizing the results obtained above, the WCCE algorithm is able to estimate the normalized covariance matrix $[C_n]$, as given by Eq. 7.1. Therefore, at this stage, two relevant issues can be considered:

- As mentioned, inversion algorithms retrieve scatterer properties from SAR data. Sometimes, these algorithms need only the complex correlation coefficients as input data, i.e., they only work with the normalized covariance matrix $[C_n]$. Consequently, the WCCE algorithm can be employed to estimate each one of the off-diagonal entries of the matrix $[C_n]$.

- If instead of $[C_n]$, interest is on the covariance matrix $[C]$, the estimation of $[C_n]$ provided by the WCCE algorithm can be understood as a first step to reduce multidimensional speckle noise in $[C]$ optimally. The multidimensional speckle noise model presented in Chapter 5 showed that the speckle's noise nature for each entry of the sample covariance matrix $[Z]$ depends on the data correlation structure. Hence, the estimated matrix $[C_n]$ can be employed to adapt the multidimensional speckle noise filter to this correlation structure.

7.4 Multidimensional Speckle Noise Filtering: Theory

The main result obtained in Chapter 5 has been the speckle noise model for the Hermitian product of a pair of SAR images, Eq. (5.95), which has been extended to multidimensional SAR imagery under the covariance matrix formulation, Eq. (5.106). Previously, in Chapter 4, a noise model for the interferometric phasor has been obtained. On the basis of this noise model, with the help of the wavelet analysis theory, a new algorithm for the estimation of the complex correlation coefficient between a pair of SAR images, in the frame of InSAR, has been proposed in Chapter 6. Previously, it has been shown that this algorithm can be extended to estimate the multidimensional SAR imagery correlation structure.

This section represents the synthesis of all the previous results with the aim to develop a new frame for multidimensional SAR speckle noise filtering. In the following section, on the basis of the results presented in Chapter 5, the linear minimum mean square error (LMMSE) filter for multidimensional SAR imagery will be presented. The availability of this filter will make possible to define new strategies to optimally filter multidimensional SAR data. Finally, important conclusions concerning multidimensional speckle filtering will be presented.

7.4.1 LMMSE Speckle Noise Filter

This section is devoted to present, on the basis of the noise model developed in Chapter 5, the LMMSE speckle noise filter for the Hermitian product of SAR images. As a consequence of data availability, the filter is developed with special emphasis to PolSAR data, despite the results which will be derived are completely valid for general multidimensional SAR imagery.

The speckle noise model for the real and imaginary parts of the Hermitian product $S_k S_l^*$, Eqs. (5.93) and (5.94), can be simplified to

$$x = \theta_1 n_m + \theta_2 + n_a \tag{7.2}$$

where θ_1 represents $\psi N_c \overline{z}_n \cos(\phi_x)$ in the real part case or $\psi N_c \overline{z}_n \sin(\phi_x)$ in the imaginary part case, θ_2 represents $\psi(|\rho| - N_c \overline{z}_n)\cos(\phi_x)$ in the real part case and $\psi(|\rho| - N_c \overline{z}_n)\sin(\phi_x)$ in the imaginary part case, n_m is the multiplicative speckle noise component, common to the real and imaginary parts and n_a represents the additive speckle components, ψn_{ar} for the real and ψn_{ai} for the imaginary part cases. Hence, the useful term to retrieve in the case of the Hermitian product real part case is

$$\theta = \theta_1 + \theta_2 = \psi N_c \overline{z}_n \cos(\phi_x) + \psi(|\rho| - N_c \overline{z}_n)\cos(\phi_x) = \psi|\rho|\cos(\phi_x) \tag{7.3}$$

whereas in the case of the imaginary part is

$$\theta = \theta_1 + \theta_2 = \psi N_c \overline{z}_n \sin(\phi_x) + \psi(|\rho| - N_c \overline{z}_n)\sin(\phi_x) = \psi|\rho|\sin(\phi_x). \tag{7.4}$$

The LMMSE filter estimates the value of θ, i.e., $\widehat{\theta}$, from the corrupted measurements given by Eq. (7.2). On the one hand, the LMMSE is based on the minimization of the mean square error (MSE) between the estimated $\widehat{\theta}$ and the actual value θ

$$MSE = E\left\{(\theta - \widehat{\theta})^2\right\} \tag{7.5}$$

under the constraint that the estimator is a linear function with respect to measured data

$$\widehat{\theta} = \sum_{n=0}^{N-1} a_n x[n] + a_N \tag{7.6}$$

where $\{a_k\}_{k=0,\ldots,N}$ are the filter coefficients. The expression of the LMMSE filter has been widely derived in literature, as for instance [173],

$$\widehat{\theta} = E\{\theta\} + \mathcal{C}_{\theta\mathbf{x}}\mathcal{C}_{\mathbf{xx}}^{-1}(\mathbf{x} - E\{\mathbf{x}\}) \tag{7.7}$$

where $\mathbf{x}$ represents the measurements vector, $\mathcal{C}_{\theta\mathbf{x}}$ is the 1 by N cross-covariance vector between θ and $\mathbf{x}$ and $\mathcal{C}_{\mathbf{xx}}$ is the N by N covariance matrix of $\mathbf{x}$. Owing to the high spatial resolution properties of SAR imagery, the image pixels can be considered uncorrelated. Hence, Eq. (7.7) simplifies to

$$\widehat{\theta} = E\{\theta\} + \frac{\mathcal{C}_{\theta x}}{\mathrm{var}\{x\}}(x - E\{x\}) \tag{7.8}$$

where $\mathcal{C}_{\theta x}$ is the covariance of the terms θ and x and $\mathrm{var}\{x\}$ is the variance of x.

The expression of the covariance term $\mathcal{C}_{\theta x}$ can be derived with the help of the noise model given by Eq. (7.2). Hence,

$$\mathcal{C}_{\theta x} = E\{(\theta - \overline{\theta})(x - \overline{x})\} = E\{\theta x\} - \overline{\theta}\overline{x} = E\{\theta x\} - \overline{\theta}^2 \tag{7.9}$$

where from Eq. (7.2) it follows $\overline{\theta} = \overline{x}$. $\overline{\theta}$ and $\overline{x}$ represent the mean values of θ and x, respectively. Considering Eq. (7.2)

$$\begin{aligned} E\{\theta x\} - \overline{\theta}^2 &= E\{\theta_1^2 n_m + \theta_1\theta_2 + \theta_1 n_a + \theta_1\theta_2 n_m + \theta_2^2 + \theta_2 n_a - \overline{\theta}_1^2 - \overline{\theta}_2^2 - 2\overline{\theta}_1\overline{\theta}_2\} \\ &= E\{\theta_1^2 n_m - \overline{\theta}_1^2 + \theta_2^2 - \overline{\theta}_2^2 + \theta_1\theta_2 + \theta_1\theta_2 n_m - 2\overline{\theta}_1\overline{\theta}_2\} + E\{\theta n_a\}. \end{aligned} \tag{7.10}$$

Since the noise term n_m is independent from useful signal θ, and $E\{n_m\} = 1$, it follows

$$\begin{aligned} E\{\theta x\} - \overline{\theta}^2 &= E\{\theta_1^2 - \overline{\theta}_1^2 + \theta_2^2 - \overline{\theta}_2^2 + 2\theta_1\theta_2 - 2\overline{\theta}_1\overline{\theta}_2\} + E\{\theta n_a\} \\ &= E\left\{((\theta_1 + \theta_2) - (\overline{\theta}_1 + \overline{\theta}_2))^2\right\} + E\{\theta n_a\} = E\{(\theta - \overline{\theta})^2\} + E\{\theta n_a\} \\ &= \mathrm{var}\{\theta\} + E\{\theta n_a\}. \end{aligned} \tag{7.11}$$

Introducing Eq. (7.11) into Eq. (7.8), the LMMSE filter expression takes the form

$$\widehat{\theta} = E\{\theta\} + \frac{\mathrm{var}\{\theta\} + E\{\theta n_a\}}{\mathrm{var}\{x\}}(x - E\{x\}). \tag{7.12}$$

Eq. (7.12) is very similar to the LMMSE filter presented by J.S. Lee *et al.* in [1], except for the term $E\{\theta n_a\}$. The authors in [1] extend the multiplicative speckle noise model of the covariance matrix diagonal elements to the off-diagonal elements. Hence, the additive noise component of speckle noise is not considered.

The terms $E\{\theta\}$, $\mathrm{var}\{\theta\}$ and $E\{\theta n_a\}$ must be estimated from measured data in order to apply the filter given by Eq. (7.12). The value of $\mathrm{var}\{\theta\}$ can be derived from $\mathrm{var}\{x\}$. On the basis of Eq. (7.2)

$$\begin{aligned} \mathrm{var}\{x\} &= E\{(x - \overline{x})^2\} = E\{(\theta_1 n_m + \theta_2 + n_a - (\overline{\theta}_1 + \overline{\theta}_2))^2\} = E\{(\theta_1 n_m + \theta_2 + n_a)^2\} - (\overline{\theta}_1 + \overline{\theta}_2)^2 \\ &= E\{\theta_1^2 n_m^2 + \theta_2^2 + n_a^2 + 2\theta_2 n_a + 2\theta_1\theta_2 n_m + 2\theta_2 n_m n_a\} - (\overline{\theta}_1 + \overline{\theta}_2)^2 \\ &= E\{\theta_1^2\}E\{n_m^2\} + E\{\theta_2^2\} + E\{n_a^2\} + 2E\{\theta_2 n_a\} + 2E\{\theta_1\theta_2\}E\{n_m\} \\ &+ E\{2\theta_2 n_a\}E\{n_m\} - (\overline{\theta}_1 + \overline{\theta}_2)^2 \end{aligned} \tag{7.13}$$

where the multiplicative noise component has been considered independent from useful signal. Introducing $E\{n_m^2\} = \mathrm{var}\{n_m\} + 1$ into Eq. (7.13) and reordering the different terms

$$\begin{aligned} \mathrm{var}\{x\} &= \underbrace{(\mathrm{var}\{\theta_1\} + E^2\{\theta_1\})(\mathrm{var}\{n_m\} + 1)}_{Mult.\ noise} + \underbrace{\mathrm{var}\{\theta_2\} + E^2\{\theta_2\} + \mathrm{var}\{n_a\}}_{Add.\ noise} \\ &+ \underbrace{2E\{\theta_1 n_a\} + 2E\{\theta_1\theta_2\}}_{Correlation\ terms} - (\overline{\theta}_1 + \overline{\theta}_2)^2 \end{aligned} \tag{7.14}$$

where the contributions of each speckle noise term have been indicated. Respect to the values of θ_1 and θ_2, in Chapter 5 it was demonstrated that the value of θ_1 is clearly larger than θ_2, compare Figs. 5.3 and 5.6. In order to facilitate the analysis of Eq. (7.14), this fact will be also translated to the variance

considering that $\text{var}\{\theta_1\} > \text{var}\{\theta_2\}$, i.e., $\text{var}\{\theta\} \simeq \text{var}\{\theta_1\}$. Introducing also $\text{var}\{\theta\} = \text{var}\{\theta_1\} + \text{var}\{\theta_2\} + 2E\{\theta_1\theta_2\} - 2\overline{\theta}_1\overline{\theta}_2$, Eq. (7.14) can be written

$$\text{var}\{x\} \simeq \text{var}\{\theta\}(1 + \text{var}\{n_m\}) + \overline{\theta}_1^2\text{var}\{n_m\} + \text{var}\{n_a\} + 2E\{\theta_1 n_a\} \tag{7.15}$$

from where it follows

$$\text{var}\{\theta\} \simeq \frac{\text{var}\{x\} - \overline{\theta}_1^2\text{var}\{n_m\} - \text{var}\{n_a\} - 2E\{\theta_1 n_a\}}{1 + \text{var}\{n_m\}}. \tag{7.16}$$

In the second and the fourth addends of the numerator, $\overline{\theta}_1$ has not been substituted by $\overline{\theta}$ in order to emphasize that the multiplicative speckle noise term do not affect the complete signal $\overline{\theta}$, but only $\overline{\theta}_1$. Introducing $E\{\theta\} = E\{x\}$ and Eq. (7.16) into Eq. (7.12), the LMMSE filter is finally

$$\widehat{\theta} = E\{\theta\} + \left[\frac{\text{var}\{x\} - \overline{\theta}_1^2\text{var}\{n_m\}}{\text{var}\{x\}(1 + \text{var}\{n_m\})} - \frac{\text{var}\{n_a\}}{\text{var}\{x\}(1 + \text{var}\{n_m\})} - \frac{E\{\theta_1 n_a\}}{\text{var}\{x\}}\left(\frac{1 - \text{var}\{n_m\}}{1 + \text{var}\{n_m\}}\right)\right](x - E\{x\}). \tag{7.17}$$

The expression of the LMMSE filter given by Eq. (7.17) is very similar to the LMMSE filter proposed by J.S. Lee *et al.* in [1]

$$\widehat{\theta} = E\{\theta\} + \left[\frac{\text{var}\{x\} - \overline{\theta}^2\text{var}\{n_m\}}{\text{var}\{x\}(1 + \text{var}\{n_m\})}\right](x - E\{x\}). \tag{7.18}$$

The difference between the LMMSE filter expressions given by Eqs. (7.17) and (7.18) lies in the fact that the authors in [1] consider that speckle noise is completely multiplicative for all the covariance matrix elements. Hence, any term accounting for the additive speckle noise components appears in Eq. (7.18). Since a fully multiplicative speckle model is not able to explain all the variance present in the measure signal x, the LMMSE filter based on this assumption, Eq. (7.18), results in signal underfiltering. This effect can be clearly observed with an example. Let the Hermitian product of two homogeneous SAR be characterized by a low coherence value. Thus, the real and imaginary parts to retrieve present low values, i.e., $\theta_1 \simeq 0$ and $\theta_2 \simeq 0$. Under this assumption, in the case of single-look imagery, which produces $E\{n_m\} = 1$, the filter's control parameter in the case of Eq. (7.18) equals

$$\frac{\text{var}\{x\} - \overline{\theta}_1^2}{2\text{var}\{x\}} \simeq \frac{1}{2}. \tag{7.19}$$

As a result, the recovered signal is $\widehat{\theta} = (1/2)E\{\theta\} + (1/2)x$. Whereas, if the complete speckle noise model is considered, the filter's control parameter in the case of Eq. (7.17) equals

$$\frac{\text{var}\{x\} - \overline{\theta}_1^2}{2\text{var}\{x\}} - \frac{\text{var}\{n_a\}}{2\text{var}\{x\}} \simeq \frac{1}{2} - \frac{1}{2} = 0 \tag{7.20}$$

producing the recovered signal to be, in this case, $\widehat{\theta} = E\{x\}$. In those situations in which the signal presents inhomogeneities, as for instance the border between two homogeneous areas or in the case of a point scatterer, the value of $\text{var}\{\theta\}$ is high, producing the retrieved value to be $\widehat{\theta} = x$ for Eqs. (7.17) and (7.18).

Until this point, only one element of the covariance matrix has been considered to be filtered by the LMMSE filter, Eq. (7.17). On the contrary, if all the covariance matrix entries are taken into account, important questions have to be addressed. The LMMSE filter given by Eq. (7.17) is completely valid to filter multidimensional SAR data under the covariance formulation. In the case of the diagonal elements, since speckle only has a multiplicative behavior, see Section 5.4.6 for details, the LMMSE filter given by Eq. (7.17) reduces to Eq. (7.18). On the other hand, in the case of the off-diagonal covariance matrix elements, the LMMSE filter proposed in this text accounts also for the additional additive speckle noise term. As it has been demonstrated in Chapter 5, the variance of the additive speckle noise term depends

on the coherence value. Consequently, since the properties of speckle noise vary between the different off-diagonal terms of the covariance matrix, the LMMSE process these elements differently. As it will be demonstrated in the following, the fact to process the elements of the covariance matrix in a different way does not damage polarimetric information, provided that this differential processing is performed in accordance with the multidimensional speckle noise model developed in Chapter 5.

The main conclusion which can be extracted from the LMMSE filter, Eq. (7.17), is that the optimum speckle noise reduction for the real and imaginary parts of the Hermitian product of a pair of SAR images has to be performed according to the complex correlation coefficient which characterizes the product. Nevertheless, the direct use of the LMMSE filter presents some drawbacks, since, on the one hand, the filter's parameters have to be estimated from data, and, on the other hand, Eq. (7.17) has been derived on the basis of several approximations. The following sections present an alternative to filter multidimensional SAR data, partially based on the LMMSE approach presented in this section.

7.4.2 Speckle Noise Terms Separation

The main result derived in Chapter 5 has been the definition of a speckle noise model for the Hermitian product of two correlated SAR images, Eq. (5.95). As demonstrated, the final speckle noise nature, resulting from the combination of a multiplicative and an additive noise term, depends on the complex correlation coefficient which characterizes this Hermitian product. In the previous section, the LMMSE filter for the Hermitian product speckle noise model has been derived. Since speckle noise depends on the complex correlation coefficient, the amount of filtering depends also on it. Consequently, if the LMMSE filter has to be applied to all the covariance matrix elements, the data correlation structure, i.e., the matrix $[C_n]$ as defined in Section 7.3, needs to be estimated.

The direct application of the LMMSE filter proposed in the previous section, Eq. (7.17), presents the drawback that some parameters have to be estimated from measured data. Considering Eq. (7.17), the parameters to estimate in the case of single-look SAR imagery are: $\mathrm{var}\{x\}$, $\overline{\theta}_1$ and $\mathrm{var}\{n_a\}$. The estimation of $\mathrm{var}\{x\}$ does not represent a problem as it is the variance corresponding to measured data. On the contrary, the estimation of the parameters $\overline{\theta}_1$ and $\mathrm{var}\{n_a\}$ needs the complex correlation coefficient ρ and the average power ψ to be estimated for every covariance matrix element. Hence, in the next section, an alternative algorithm to retrieve the true covariance matrix from measured multidimensional SAR data, i.e., from $[Z]$, is proposed and studied. The basis of this algorithm consists in a pre-processing step which eliminates the additive speckle noise term from all the elements of the covariance matrix and filters the multiplicative part with standard approaches.

As proved in Section 5.4.7, the true covariance matrix $[C]$ can be divided into two additional matrices $[C_1]$ and $[C_2]$. The multiplicative speckle noise term only corrupts the elements of the matrix $[C_1]$, to which the matrix $[C_2]$ and the additive speckle noise term are added, see Eq. (5.106) and Section 5.4.7 for details. As demonstrated in Chapter 5, the matrix $[C_1]$ contains the majority of the signal in $[C]$, whereas the matrix $[C_2]$ contains only a small portion of it. In order to validate the speckle noise model for the Hermitian product, it was divided into two components. A multiplicative part containing the information of the entries of $[C_1]$, damaged by the multiplicative speckle noise component and an additive part containing the elements of $[C_2]$ plus the additive speckle noise component, see Eq. (5.109). Considering PolSAR data, let $S_{pq}S_{rs}^*$ be the Hermitian product of a pair of PolSAR images referred to the linear polarization basis $\{\widehat{\mathbf{h}}, \widehat{\mathbf{v}}\}$, hence, the two terms of the Hermitian product are

$$Multiplicative\ Term \quad \Rightarrow \quad \psi N_c \overline{z}_n n_m \exp(j\phi_x) \tag{7.21}$$

$$Additive\ Term \quad \Rightarrow \quad \psi(|\phi| - N_c\overline{z}_n)\exp(j\phi_x) + \psi(n_{ar} + jn_{ai}). \tag{7.22}$$

This division can be performed for each covariance matrix element. But, as it was also seen throughout all the Chapter 5, this division depends on the complex correlation coefficient characterizing every

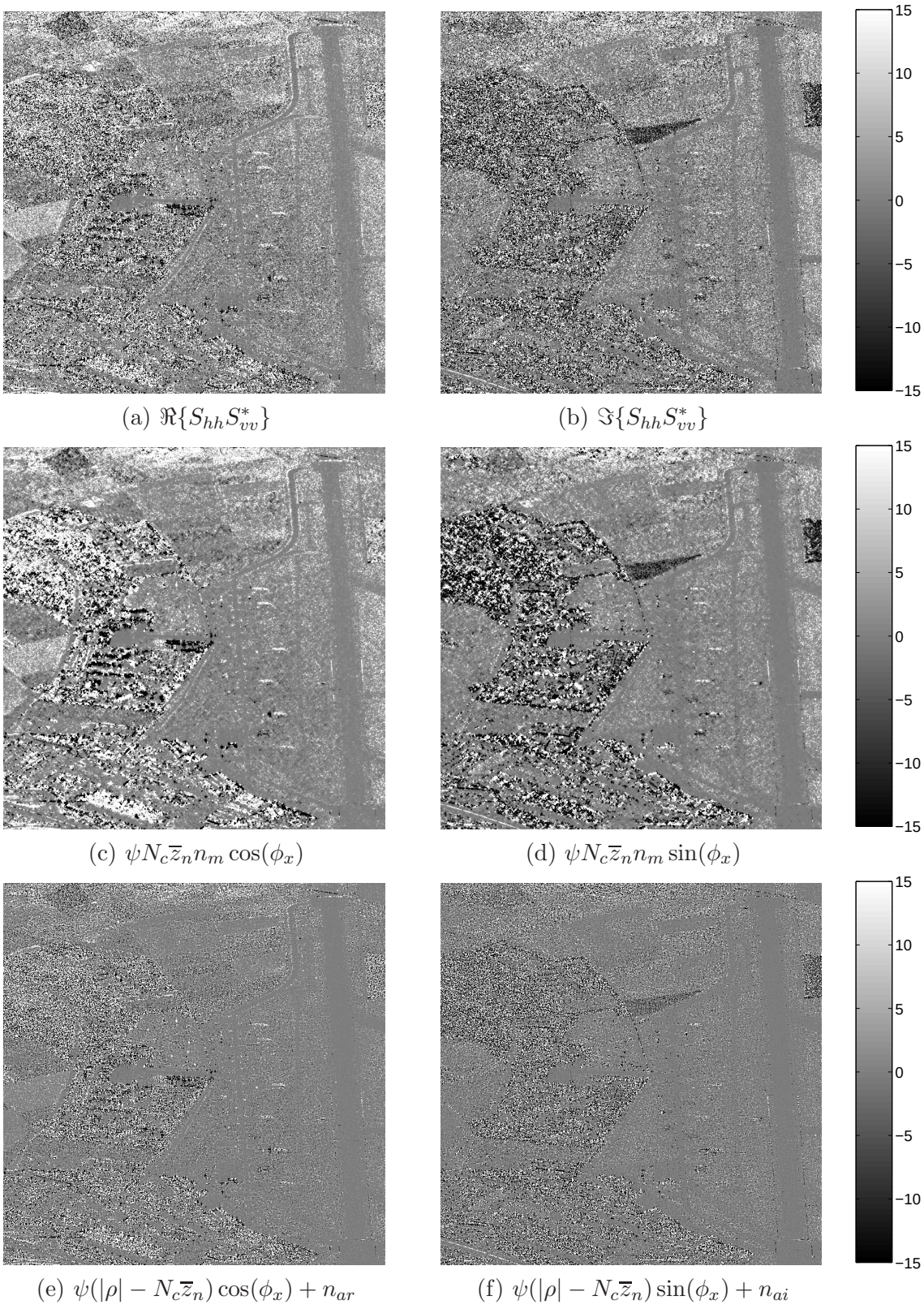

(a) $\Re\{S_{hh}S_{vv}^*\}$ (b) $\Im\{S_{hh}S_{vv}^*\}$

(c) $\psi N_c \overline{z}_n n_m \cos(\phi_x)$ (d) $\psi N_c \overline{z}_n n_m \sin(\phi_x)$

(e) $\psi(|\rho| - N_c\overline{z}_n)\cos(\phi_x) + n_{ar}$ (f) $\psi(|\rho| - N_c\overline{z}_n)\sin(\phi_x) + n_{ai}$

Figure 7.10: Noise components of the real and imaginary parts of the term $S_{hh}S_{vv}^*$. (a) Hermitian product real part. (b) Hermitian product imaginary part. (c) Multiplicative term of the Hermitian product real part. (d) Multiplicative term of the Hermitian product imaginary part. (e) Additive term of the Hermitian product real part. (f) Additive term of the Hermitian product imaginary part.

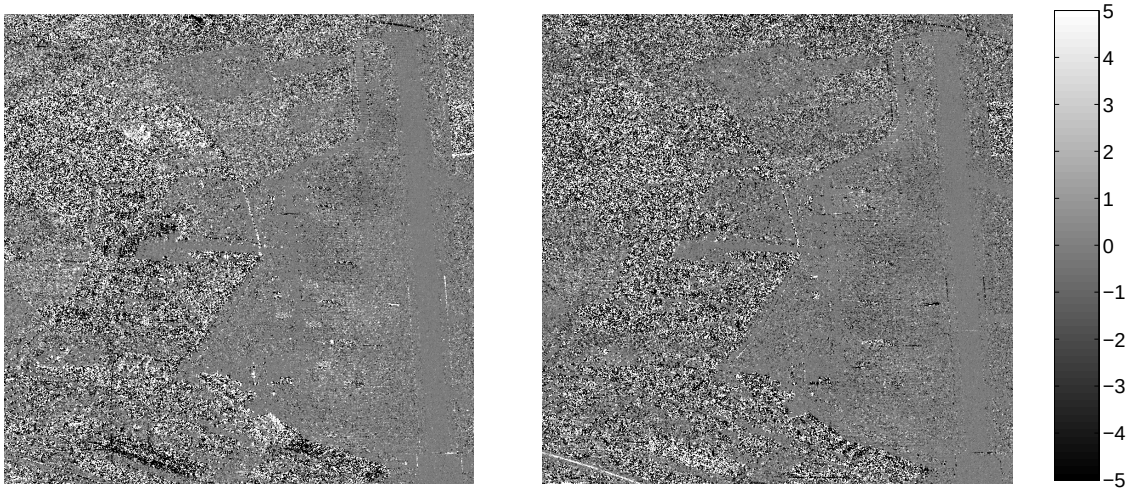

(a) $\Re\{S_{hh}S_{hv}^*\}$ (b) $\Im\{S_{hh}S_{hv}^*\}$

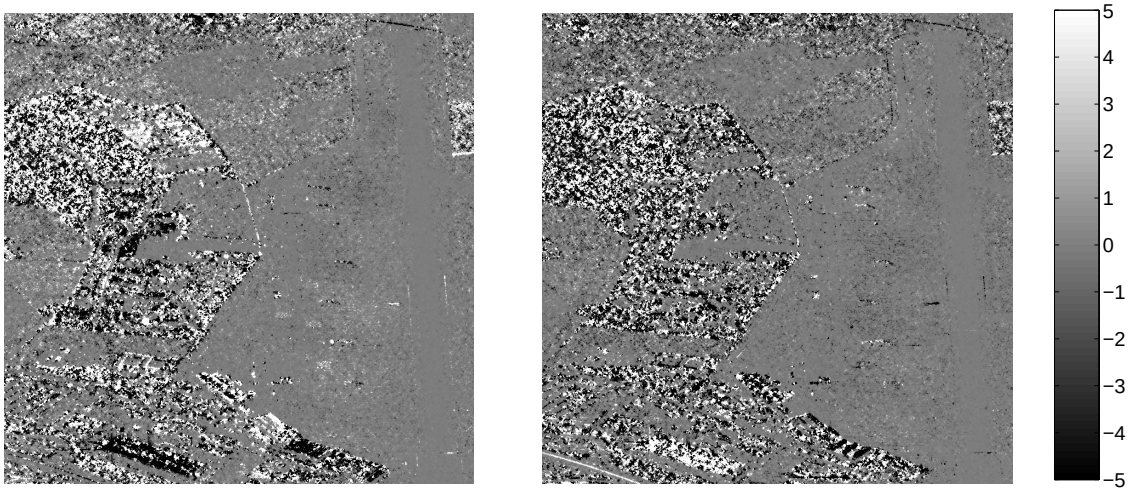

(c) $\psi N_c\overline{z}_n n_m \cos(\phi_x)$ (d) $\psi N_c\overline{z}_n n_m \sin(\phi_x)$

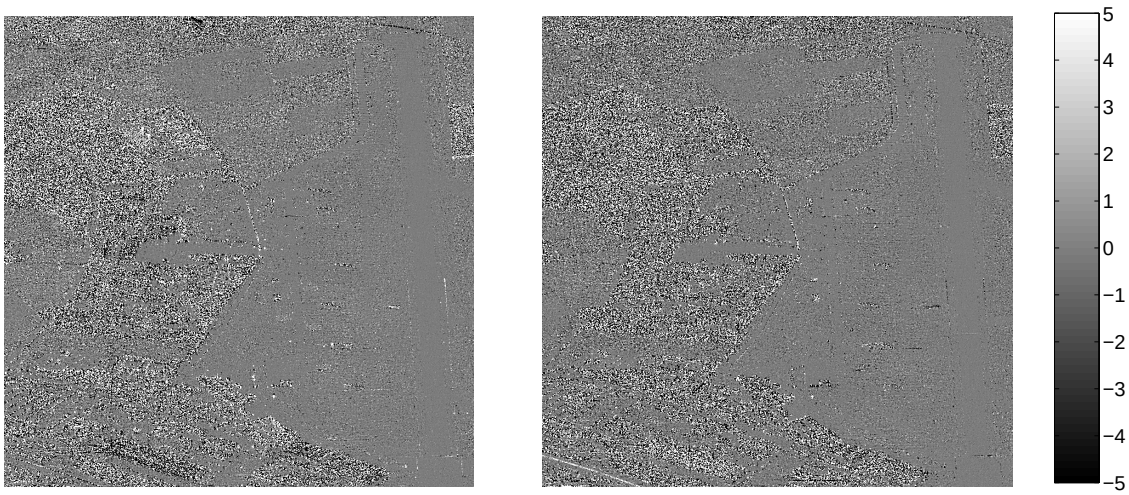

(e) $\psi(|\rho| - N_c\overline{z}_n)\cos(\phi_x) + n_{ar}$ (f) $\psi(|\rho| - N_c\overline{z}_n)\sin(\phi_x) + n_{ai}$

Figure 7.11: Noise components of the real and imaginary parts of the term $S_{hh}S_{hv}^*$. (a) Hermitian product real part. (b) Hermitian product imaginary part. (c) Multiplicative term of the Hermitian product real part. (d) Multiplicative term of the Hermitian product imaginary part. (e) Additive term of the Hermitian product real part. (f) Additive term of the Hermitian product imaginary part.

covariance matrix element. For instance, the diagonal elements are characterized by presenting only the multiplicative speckle term. From what is has been presented in Section 5.4.1, Eqs. (5.25) and (5.26), and considering Section 5.5.1, it is easy to separate the multiplicative and the additive terms for each element of the covariance matrix $[C]$. In Section 7.3.1 it was demonstrated that the WCCE can estimate the parameter $N_c \exp(j\phi_x)$. Hence, if z is the amplitude of $S_{pq}S^*_{rs}$, it is easy to conclude that the two terms of the Hermitian product can be obtained as

$$Multiplicative\ Term \Rightarrow zN_c \exp(j\phi_x) \tag{7.23}$$

$$Additive\ Term \Rightarrow S_{pq}S^*_{rs} - zN_c \exp(j\phi_x). \tag{7.24}$$

In Section 7.3.2, the WCCE algorithm has been employed to estimate the modulated coherence term $N_c \exp(j\phi_x)$ corresponding to the covariance matrix elements $S_{hh}S^*_{vv}$ and $S_{hh}S^*_{hv}$ of a fully polarimetric L-band (1.3 GHz) dataset of the Oberpfaffenhofen test site, acquired with the E-SAR system. Hence, the multiplicative and the additive terms of the covariance matrix entries $S_{hh}S^*_{vv}$ and $S_{hh}S^*_{hv}$ have been calculated with Eqs. (7.23) and (7.24). The corresponding results are presented respectively by Figs. 7.10 and 7.11.

From Figs. 7.10 and 7.11, several points can be observed. First of all, one can notice that most of the information contained in the original images, Figs. 7.10a and 7.10b for $S_{hh}S^*_{vv}$ and Figs. 7.11a and 7.11b for $S_{hh}S^*_{hv}$, is concentrated on the multiplicative signal terms, whereas the additive terms are basically noise. In addition, the figures corresponding to the additive terms Figs. 7.10e and 7.10f for $S_{hh}S^*_{vv}$ and Figs. 7.11e and 7.11f for $S_{hh}S^*_{hv}$, are non-homogeneous. If the coherence maps shown in Section 7.3.2 for each covariance matrix element are considered, one can observe that the larger variance for the additive term correspond to those areas with the lower covariance values. Hence, it can be concluded, that the separation of the Hermitian product real and imaginary parts induced by Eqs. (7.23) and (7.24) can be considered as a PolSAR data filter as it eliminates the additive speckle noise term. On the one hand, this approach maintains the spatial properties of the original images thanks to the use of the WCCE algorithm to estimate the correlation structure. On the other hand, it is adaptive in the sense that it eliminates the additive term on the basis of the correlation structure. Hence, in order to have a complete speckle noise reduction, the multiplicative speckle components has to be filtered out. As it will be shown, the information of N_c is recovered instead $|\rho|$, making necessary a last processing step to invert this effect.

A point which has been addressed through all this text is the maintenance of the spatial properties and the spatial details, whenever a signal is processed. Consequently, the step to separate the real and the imaginary parts of the Hermitian product in the corresponding multiplicative and additive terms is specially sensitive to a possible loss of spatial resolution, depending on the data employed to split the Hermitian product. As it has been demonstrated, the WCCE algorithm possess enviable properties to estimate the modulated coherence term, which is employed to split the Hermitian product real and imaginary parts. In Figs. 7.2a and 7.2b two areas of 256 by 256 pixels were marked with red squares. The separation of the Hermitian product into the multiplicative and the additive terms is now analyzed in these areas to study the spatial properties of the separated signals. Fig. 7.12 contains the detail images of the different components obtained from the separation of the product $S_{hh}S^*_{vv}$. The coherence and the phase information derived with the WCCE algorithm can be observed in Figs. 7.4b and 7.5c. As it can be observed in Fig. 7.12, the multiplicative and the additive term present practically the same spatial resolution as the original images. Additionally two details must be mentioned. As observed from the coherence map, Fig. 7.4b, the high coherence detail on the upper left-hand side corner, characterized by an average phase difference of approximately 0 rad as given by Fig. 7.5c, produces this area to be mainly concentrated on the multiplicative term of the real part of the Hermitian product. On the contrary, if one looks to the low coherence area crossing the lower part of the coherence map, Fig. 7.4b, this is almost concentrated on the additive term of the Hermitian product.

Fig. 7.13 contains the detail images of the different components obtained from the separation of the product $S_{hh}S^*_{hv}$, for the areas marked with red squares in Figs. 7.6a and 7.6b. The coherence and the

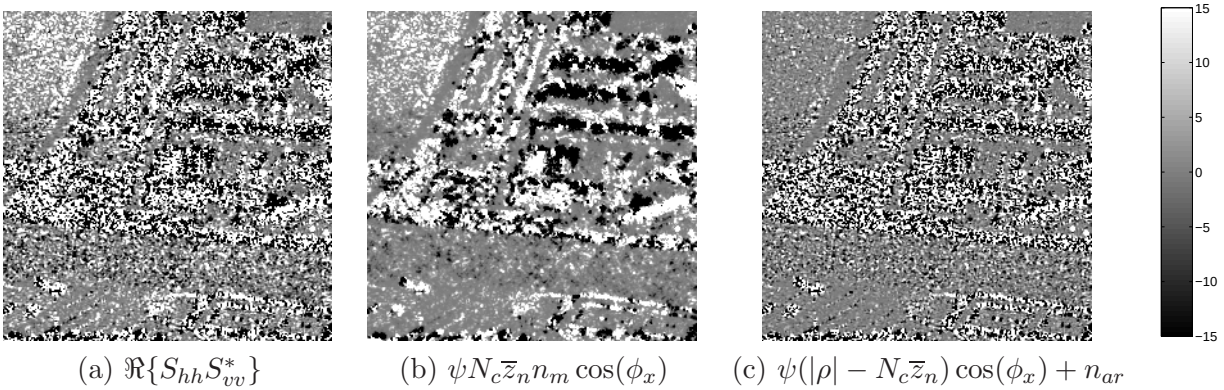

(a) $\Re\{S_{hh}S_{vv}^*\}$ (b) $\psi N_c\overline{z}_n n_m \cos(\phi_x)$ (c) $\psi(|\rho| - N_c\overline{z}_n)\cos(\phi_x) + n_{ar}$

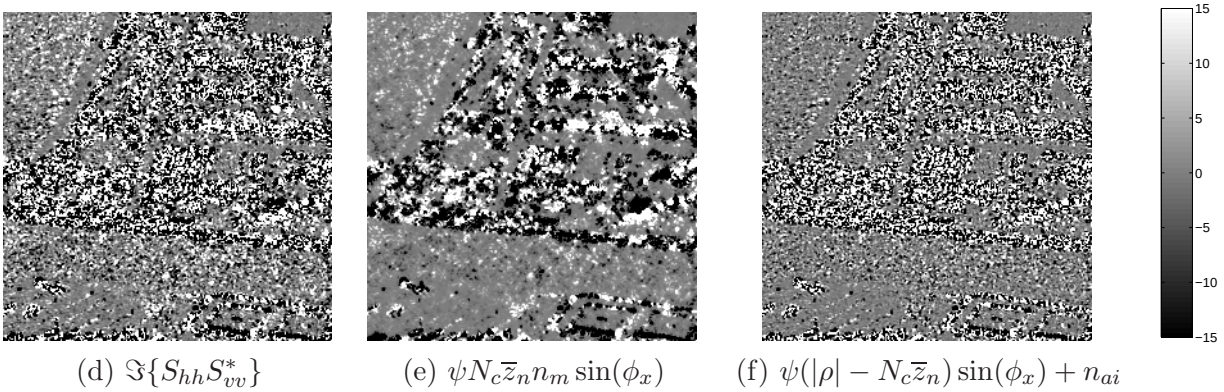

(d) $\Im\{S_{hh}S_{vv}^*\}$ (e) $\psi N_c\overline{z}_n n_m \sin(\phi_x)$ (f) $\psi(|\rho| - N_c\overline{z}_n)\sin(\phi_x) + n_{ai}$

Figure 7.12: Detail images for the noise components of the real and imaginary parts of the term $S_{hh}S_{vv}^*$. (a) Hermitian product real part. (b) Hermitian product real part multiplicative term. (c) Hermitian product real part additive term. (d) Hermitian product imaginary part. (e) Hermitian product imaginary part multiplicative term. (f) Hermitian product imaginary part additive term.

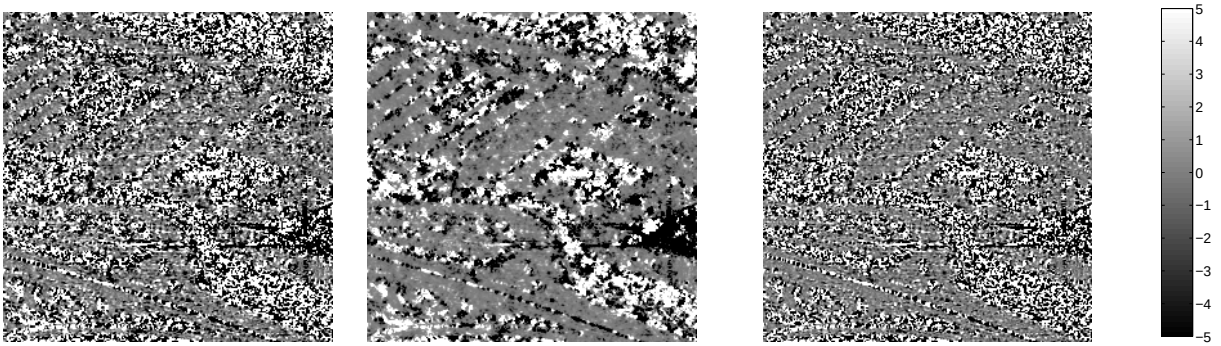

(a) $\Re\{S_{hh}S_{hv}^*\}$ (b) $\psi N_c\overline{z}_n n_m \cos(\phi_x)$ (c) $\psi(|\rho| - N_c\overline{z}_n)\cos(\phi_x) + n_{ar}$

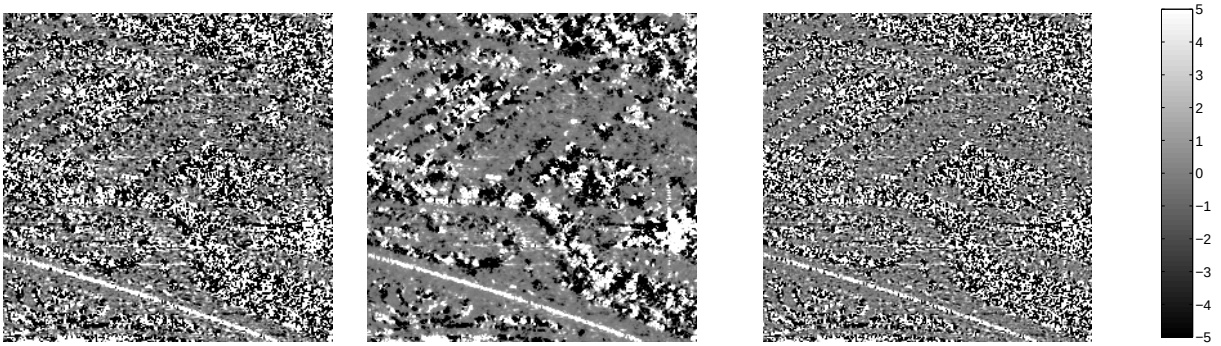

(d) $\Im\{S_{hh}S_{hv}^*\}$ (e) $\psi N_c\overline{z}_n n_m \sin(\phi_x)$ (f) $\psi(|\rho| - N_c\overline{z}_n)\sin(\phi_x) + n_{ai}$

Figure 7.13: Detail images for the noise components of the real and imaginary parts of the term $S_{hh}S_{hv}^*$. (a) Hermitian product real part. (b) Hermitian product real part multiplicative term. (c) Hermitian product real part additive term. (d) Hermitian product imaginary part. (e) Hermitian product imaginary part multiplicative term. (f) Hermitian product imaginary part additive term.

phase information derived with the WCCE algorithm can be observed in Figs. 7.8b and 7.9c. In this case, the effect of the separation is more severe since the term $S_{hh}S_{hv}^{*}$ is characterized by lower coherences than $S_{hh}S_{vv}^{*}$. Again, it can be observed that the separated signal components practically do not have a loss on spatial resolution with respect to the original images. This is highly noticeable in the straight line detail, corresponding to the separation of two lanes in a highway crossing the lower left-hand corner of the images.

As it can be deduced from the previous results, the capability of the WCCE algorithm to estimate the correlation structure, which at the same time allows to split the covariance matrix $[C]$ into the multiplicative term, i.e., $[N_m]\mathbf{c}_1$ in Eq. (5.106), and the additive term, i.e., $\mathbf{c}_2 + \mathbf{n}_a$ in Eq. (5.106), permits, as it will be shown, an optimum speckle noise reduction in multidimensional SAR data.

7.4.3 Multidimensional Speckle Noise Reduction: Algorithm

The direct use of the LMMSE filter developed for the multidimensional speckle noise model, Eq. (7.17), needs the estimation of several signal parameters. In order to avoid the estimation of these parameters, an alternative algorithm to filter multidimensional SAR imagery, under a covariance matrix formulation, is proposed in the following [212]. Sice the Hermitian product of a pair of SAR images is affected by two different noise sources, the algorithm which is next proposed will reduce them in a two step process. First, the data's correlation structure is estimated in order to separate both noise components. From these two, the additive term will be discarded, whereas the multiplicative one is filtered by standard filters. If is worth to mention that the final effect of this algorithm is to filter the off-diagonal elements of the covariance matrix differently, but as it will be demonstrated, this does not represent a destruction of the polarimetric information. In the following, a step-by-step description of this algorithm is given, whereas an scheme is presented by Fig. 7.14.

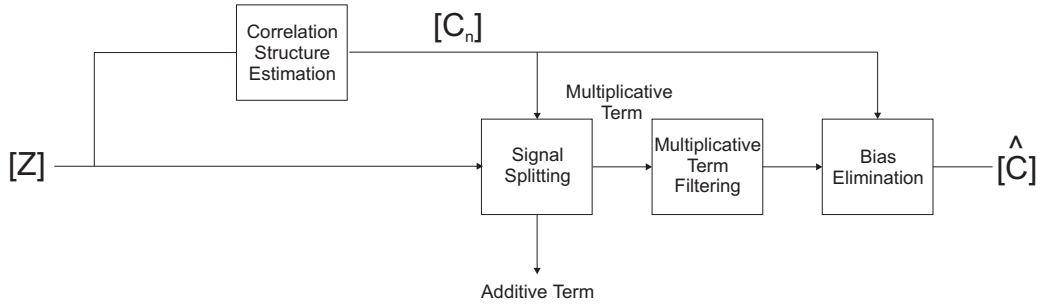

Figure 7.14: Scheme of the multidimensional speckle noise reduction algorithm. In this case, the scheme is particularized for PolSAR data.

Step 1: *Correlation structure estimation.* This step consists in the estimation of the multidimensional data's correlation information in order to separate the multiplicative and the additive noise terms of the Hermitian product. To perform this task, several procedures can be employed. A first option is to do it through a multilook process, which leads to a loss of spatial resolution. A second alternative is to estimate this information by means of the WCCE algorithm. As shown in Section 7.3, this procedure maintains the spatial properties of the input signal. The estimation of the complex correlation coefficients has to be applied only over the off-diagonal elements of the covariance matrix, since the diagonal elements are characterized by a complex correlation coefficient equal to 1. In the case of the off-diagonal elements, the modulated coherence, i.e., $N_c \exp(j\phi_x)$, must be estimated instead of the complex correlation coefficient, since the former allows to split the Hermitian products into the multiplicative and the additive terms.

Step 2: *Data splitting.* Once the correlation structure of multidimensional SAR data is estimated, the procedure detailed in Section 7.4.2, i.e., Eqs. (7.23) and (7.24), is employed to split the

covariance matrix elements into the multiplicative and the additive terms. This step does not have to be applied to the diagonal elements since they are already characterized by a multiplicative speckle term. For each off-diagonal element, the additive term is discarded since it is basically due to noise. The multiplicative terms are retained as they contain the major part of the signal to retrieve. The statistical properties of this term have been extensively studied in Section 5.4.1. This step can be considered as a first speckle noise reduction, since it eliminates the additive speckle term on the basis of the multidimensional SAR imagery correlation structure.

Step 3: *Multiplicative speckle term filtering.* This step concerns the multiplicative speckle term filtering. To perform this filtering, several alternatives can be implemented. On the one hand, the multilook filter can be employed at the expense of spatial resolution. A second approach is to filter it by the LMMSE filter as given in [1], since it is optimized for multiplicative noise. The LMMSE filter expression is given by Eq. (7.18). The filter parameters are calculated employing the local statistic filter [192] in edge-aligned windows [210]. Hence, this approach ensures the maintenance of the spatial properties of the original signal.

Step 4: *SAR data recovery.* The recovered diagonal elements from measured data correspond directly to the final values of the covariance matrix. This is not the case for the off-diagonal elements. As it can be concluded from Section 5.4.1, the recovered values obtained as a result of applying the LMMSE algorithm over the multiplicative term of the off-diagonal covariance matrix elements results in a small bias. If the Hermitian product real part is considered, the recovered mean value for the multiplicative term is given by Eq. (5.33), whereas the actual value should be Eq. (5.23). Hence, one can conclude that the bias is eliminated if each off-diagonal element recovered in the previous step is multiplied by

$$\mathcal{B} = \frac{|\rho|}{N_c \frac{\pi}{4} {}_2F_1\left(-\frac{1}{2}, -\frac{1}{2}; 1; |\rho|^2\right)}. \tag{7.25}$$

Fig. 7.15 presents a plot of the parameter $\mathcal{B}$. This parameter can be easily estimated from the obtained value of N_c. As it can be observed, the higher the coherence, the lower the influence of the additive speckle term, producing the close to one the parameter $\mathcal{B}$.

The algorithm described in the previous lines has to be understood as a general approach to filter multidimensional speckle noise, since, the procedures employed to estimate the data's correlation structure and to filter the multiplicative speckle term can vary.

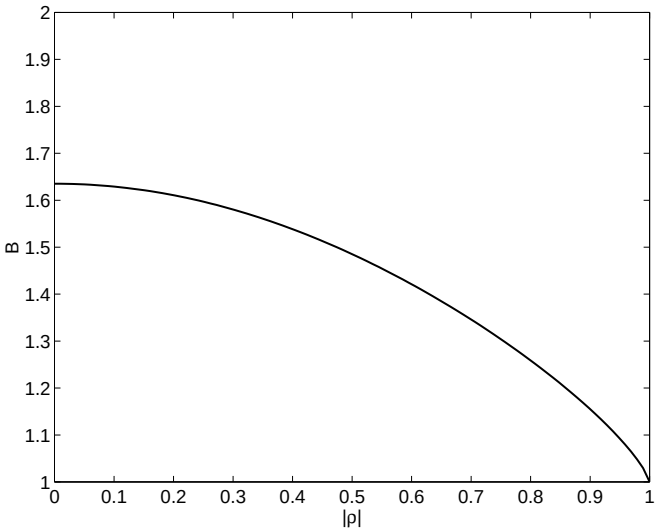

Figure 7.15: Evolution of the parameter $\mathcal{B}$ as a function of $|\rho|$.

7.5 Polarimetric Speckle Noise Reduction: Results

This section concerns the evaluation of the algorithm presented in the previous section. Specifically, this algorithm will be evaluated by means of simulated and real PolSAR data. As defined, the algorithm bases speckle noise reduction on the speckle noise model developed and validated in Chapter 5. As a result of the availability of this model, the algorithm eliminates noise in a two step process. First, it filters the additive speckle noise term on the basis of the data's correlation structure. Second, the multiplicative speckle term is reduced by standard techniques. Consequently, the algorithm filters differently each one of the covariance matrix elements, adapting to the data's correlation structure. This section will evaluate the capability of the proposed algorithm to reduce speckle noise while preserving the polarimetric properties of the input signal. Finally, the maintenance of spatial resolution will be addressed by means of real PolSAR data. Despite the algorithm is evaluated by means of PolSAR data, the conclusions which will be extracted from this analysis, can be extended to the case of any multidimensional SAR dataset.

As one can notice, the algorithm proposed in Section 7.4.3 enters in clear contradiction with two of the points mentioned in [1], also given in Section 7.2, regarding the properties a PolSAR filter should fulfill for a correct speckle noise reduction without damaging polarimetric information. The first of these points deals with the use of the coherence information in order to process data, whereas the second one has to do with the way the covariance matrix elements have to be processed. As a consequence of the results which will be presented below, these points will be redefined, allowing to extend the criteria under which a PolSAR, or a multidimensional SAR data, speckle filter has to be developed.

As explained at the beginning of this chapter, a key issue when a PolSAR filter is defined, is its ability to eliminate noise without damaging polarimetric information. Hence, the maintenance of these polarimetric properties has to be quantitatively measured in order to evaluate the filter's performance. In the next, the preservation of these properties is measured in three different ways. The covariance matrix elements are characterized by the coherence $|\rho|$ between the SAR images from which the Hermitian product is obtained. Hence, the maintenance of coherence is first examined. These quantities make reference to second order statistics, which have been shown to completely characterize multidimensional SAR data under the Gaussian scattering assumption, see Section 5.2 for details. Therefore, if the coherence information is maintained in this case, it implies the maintenance of polarimetric information. With this analysis, the elements of the covariance matrix are considered separately. As a consequence, it is worthwhile to measure the estimated covariance matrix polarimetric properties in a way considering it as a unit, and not as a collection of elements. The collective properties of the covariance matrix are considered by means of two additional approaches. On the one hand, it is studied in the frame of the eigenvector-based target decomposition techniques of the coherency matrix $[T]$ by the so-called $H/\overline{\alpha}/A$ decomposition [108, 36, 165]. On the other hand, the polarimetric properties of filtered data are studied by means of the *Polarimetric Signatures* (PS), also known as *Polarimetric Responses* [115, 16, 77].

In Chapter 2, it was shown that distributed scatterers are completely characterized, under the Gaussian scattering assumption, by means of second order statistics. Target decomposition theorems, first formalized by Huynen [28], provide the frame to study these random scatterers trough the concept of average or dominant scatterer [36]. The presence of speckle noise produces the measured data to be random, making necessary to construct the average scattering mechanism. Target decomposition techniques give the tools to provide a physical interpretation to this average scattering mechanism. Given a measured covariance matrix $[Z]$, it is necessary to estimate from it the covariance matrix $[C]$, i.e., formally defined as $[C] = E\{[Z]\}$. The most simple way to obtain an estimation of $[C]$, denoted by $[\widehat{C}]$, is to substitute the expectation operator by a spatial average, Eq. (2.180). Consequently, if any other estimation process is defined, as for instance the one given in Section 7.4.3, the estimated matrix $[\widehat{C}]$ has to maintain the average scattering mechanism properties. For this reason, the average mechanism obtained through a spatial average is assumed as a reference. The covariance matrix $[C]$ can be transformed to the coherency

matrix $[T]$, see Section 2.3.4. This new matrix can be decomposed as follows [165]

$$[T] = [U_3] \begin{bmatrix} \lambda_1 & 0 & 0 \\ 0 & \lambda_2 & 0 \\ 0 & 0 & \lambda_3 \end{bmatrix} [U_3]^{*T} \tag{7.26}$$

$$[U_3] = \begin{bmatrix} \cos(\alpha_1) & \cos(\alpha_2) & \cos(\alpha_3) \\ \sin(\alpha_1)\cos(\beta_1)e^{j\delta_1} & \sin(\alpha_2)\cos(\beta_2)e^{j\delta_2} & \sin(\alpha_3)\cos(\beta_3)e^{j\delta_3} \\ \sin(\alpha_1)\sin(\beta_1)e^{j\gamma_1} & \sin(\alpha_2)\sin(\beta_2)e^{j\gamma_2} & \sin(\alpha_3)\sin(\beta_3)e^{j\gamma_3} \end{bmatrix}. \tag{7.27}$$

Eqs. (7.26) and (7.27) represent a parameterization of the decomposition of the matrix $[T]$ into his eigenvalues, given by λ_1, λ_2 and λ_3, such that, $\lambda_1 \geq \lambda_2 \geq \lambda_3 \geq 0$, and his eigenvectors, defined as the columns of the matrix $[U_3]$. From the eigenvalues, the target entropy H (in the von Neumann sense), which measures the depolarization caused by the target, is defined as

$$H = \sum_{q=1}^{Q} -P_q \log_n P_q \quad P_q = \frac{\lambda_q}{\sum_{j=1}^{n} \lambda_j} \tag{7.28}$$

where $Q = 3$ for backscatter problems. By definition, $H \in [0, 1]$. The extreme case $H = 0$ corresponds to polarized targets, whereas $H = 1$ corresponds to random targets [36]. The $\overline{\alpha}$ angle, known as mean scattering mechanism, in the backscattering case, is defined as

$$\overline{\alpha} = P_1\alpha_1 + P_2\alpha_2 + P_3\alpha_3. \tag{7.29}$$

Finally, the anisotropy is defined as

$$A = \frac{\lambda_2 - \lambda_3}{\lambda_2 + \lambda_3}. \tag{7.30}$$

As a result, any algorithm attempting to estimate $[C]$, i.e., an algorithm reducing speckle noise, has to maintain the values of H, $\overline{\alpha}$ and A.

The second way to consider the estimated covariance matrix as a unit, consists in obtaining the Polarimetric Signature (PS) of the target. The PS is a graphical representation of the variation of the scattering cross section as a function of polarization [77]. The response consists in a plot of synthesized scattering cross section as a function of ellipticity τ and orientation ϕ angles. Two kind of signatures will be employed here: in the case of the co-polarized signatures, the transmitting and the receiving antennas have the same polarization; in the case of the cross-polarized signatures, the receiving antenna is polarized orthogonally to the transmitting antenna.

7.5.1 Polarimetric Speckle Noise Reduction: Simulated PolSAR Data

This section proves that the algorithm presented in Section 7.4.3 is able to reduce speckle noise effects and also to preserve data's polarimetric information. In order to estimate the multidimensional data's correlation structure, the multilook approach, as well as the WCCE algorithm, will be evaluated. The multiplicative filtering step will be performed by means of the multilook approach and the LMMSE filter, as given in [1]. In order to perform an accurate quantitative analysis, simulated data must be employed in order to have a complete knowledge concerning the signal to recover. Hence, the algorithm presented in Section 4.2.3, already considered to validate the Hermitian product speckle noise model, is here employed.

As proved in Chapter 5, the final speckle noise nature for multidimensional SAR data depends on the multidimensional data's correlation structure, in such a way that the Hermitian product speckle noise results from the combination of multiplicative and additive noise components. In the next, the performance of the speckle noise reduction algorithm, proposed in Section 7.4.3, is studied as a function

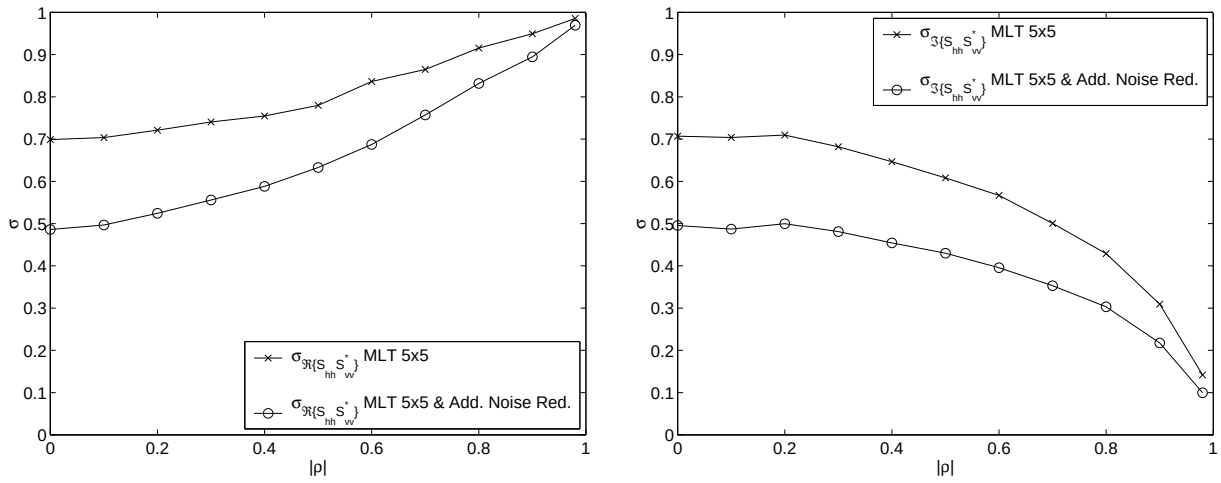

(a) $\Re\{\widehat{S_{hh}S_{vv}^*}\}$ (b) $\Im\{\widehat{S_{hh}S_{vv}^*}\}$

Figure 7.16: Standard deviations of the processed term $S_{hh}S_{vv}^*$ as a function of $|\rho|$ for the multilook (MLT) approach with and without additive noise reduction.

of coherence $|\rho|$. To perform such an analysis, a random scattering vector $\mathbf{k} = [S_{hh}\ S_{hv}\ S_{vv}]^T$ is simulated, characterized by a covariance matrix of a reflection symmetric scatterer

$$[C] = \begin{bmatrix} 5 & 0 & 5|\rho|\exp(j\phi_x) \\ 0 & 2 & 0 \\ 5|\rho|\exp(-j\phi_x) & 0 & 5 \end{bmatrix} \tag{7.31}$$

where $|\rho|\exp(j\phi_x)$ is the complex correlation coefficient which characterizes the Hermitian product $S_{hh}S_{vv}^*$. The coherence of the products $S_{hh}S_{hv}^*$ and $S_{hv}S_{vv}^*$ are supposed to be equal to zero, producing these terms to contain only additive speckle. In the case of the term $S_{hh}S_{vv}^*$, the speckle noise nature in the real part case depends on the value of $|\rho|$, whereas it is always additive in the case of the imaginary part, since $\phi_x = 0$ rad is considered.

The first analysis consists of a test to study the effects of the coherence $|\rho|$, characterizing $S_{hh}S_{vv}^*$. The simulated data has been processed with the algorithm presented in Section 7.4.3 as follows. The complex correlation coefficients of the different off-diagonal covariance matrix elements are estimated with a multilook approach employing a 5 by 5 pixel window, in order to filter the additive speckle component. This same approach is employed to reduce the effects of multiplicative noise. The fist parameter which has been considered is the standard deviation (σ) of the filtered real and imaginary parts of the covariance matrix term $S_{hh}S_{vv}^*$. Figs. 7.16a and 7.16b show the graphic plots of these values for data processed with the 5 by 5 pixel multilook approach with and without additive speckle noise reduction. A more careful look to Figs. 7.16a and 7.16b shows that the real and imaginary parts of the term $S_{hh}S_{vv}^*$, in which additive speckle noise is first reduced, present lower variances in all the coherence range, compared with the values corresponding to the standard multilook filter. Since the lower the coherence $|\rho|$, the larger the additive speckle standard deviation, one observes that larger noise reductions are obtained for low coherences. Figs. 7.16a and 7.16b confirm the fact that to process the additive speckle noise component leads to a larger reduction of speckle noise.

From a theoretical point of view, since the speckle additive noise term is first reduced, it should produce, for the simulated data case, the Hermitian product $S_{hh}S_{vv}^*$ imaginary part to present a standard deviation close to zero for all the coherence range, since speckle is completely additive. This should be also the case for low coherences in the case of the real part of $S_{hh}S_{vv}^*$. The reason of not obtaining lower variances in those cases lies, first, on the overestimation of the coherence value $|\rho|$, see Section 6.2.2. As a consequence of it, the algorithm's step performing the additive speckle noise reduction attenuates this noise component less than it should correspond. The second reason explaining this lower additive

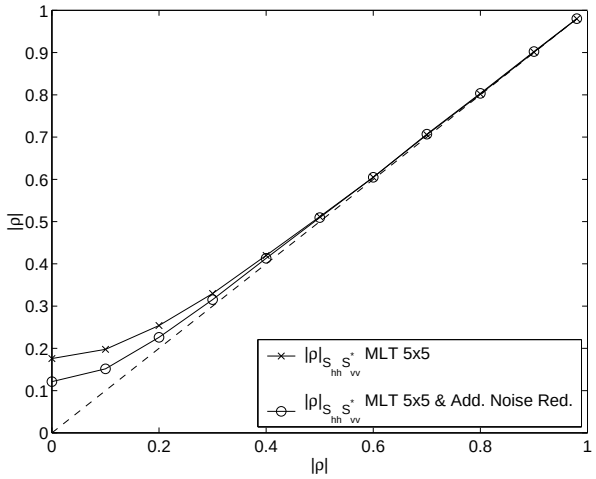

Figure 7.17: Coherence estimated for the processed term $S_{hh}S_{vv}^{*}$ as a function of $|\rho|$ for the multilook (MLT) approach with and without additive noise reduction.

speckle noise reduction is a consequence of the properties of the estimated phase difference $\widehat{\phi}_x$. For low coherences, the phase difference is almost uniformly distributed, making complex to derive a reliable estimated values. Despite these facts, as shown in Figs. 7.16a and 7.16b, even in those cases in which the estimation of a reliable complex coefficient term is difficult, the algorithm proposed in Section 7.4.3, is able to provide a larger noise reduction, if compared with a standard noise reduction technique, thanks to the reduction of a part of the additive speckle term.

The additional standard deviation reduction coming from the elimination of the additive speckle term, based on coherence, does not damage data's polarimetric information. The first parameter which has been analyzed, in this sense, is the coherence value estimated from processed data. Fig 7.17 presents the estimated coherence value from data filtered with a standard multilook without eliminating the additive speckle noise and with the algorithm given in Section 7.4.3. As it can be concluded from Fig. 7.17, the removal of the additive speckle term as a function of coherence, does not alter it at final data. In this case, one can observe that the elimination of the additive speckle term, on the contrary, decreases the coherence bias as a result of the minor noise content. Hence, the additional reduction of the additive speckle term makes the proposed algorithm to increase the accuracy of the estimated coherence with

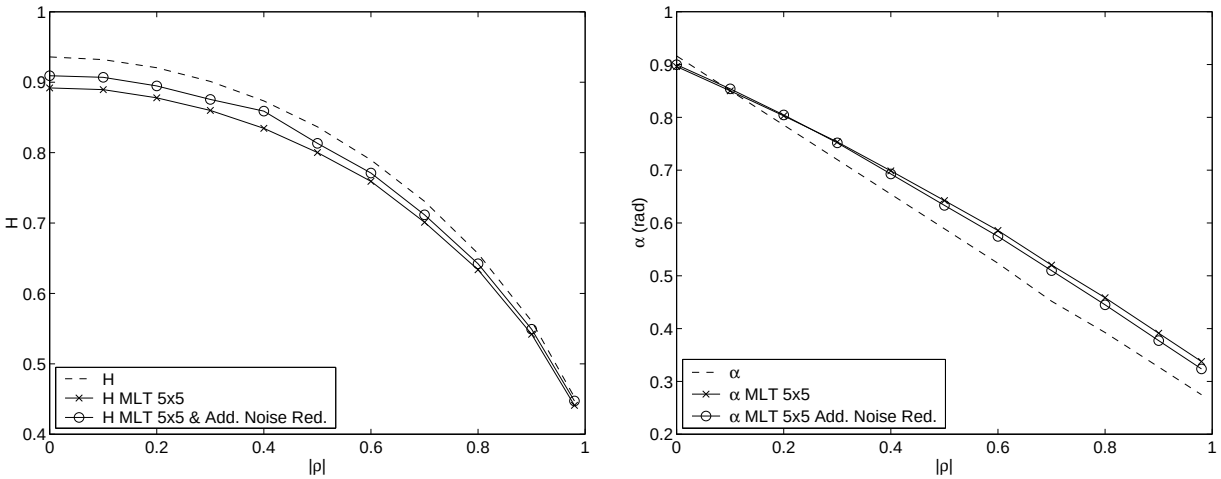

(a) H (b) $\overline{\alpha}$

Figure 7.18: Entropy H and $\overline{\alpha}$ values estimated from processed data. Dashed lines represent theoretical values of these two parameters of the covariance matrix defined as given by Eq. (7.31), for $|\rho| \in [0, 1]$ and $\phi_x = 0$ rad.

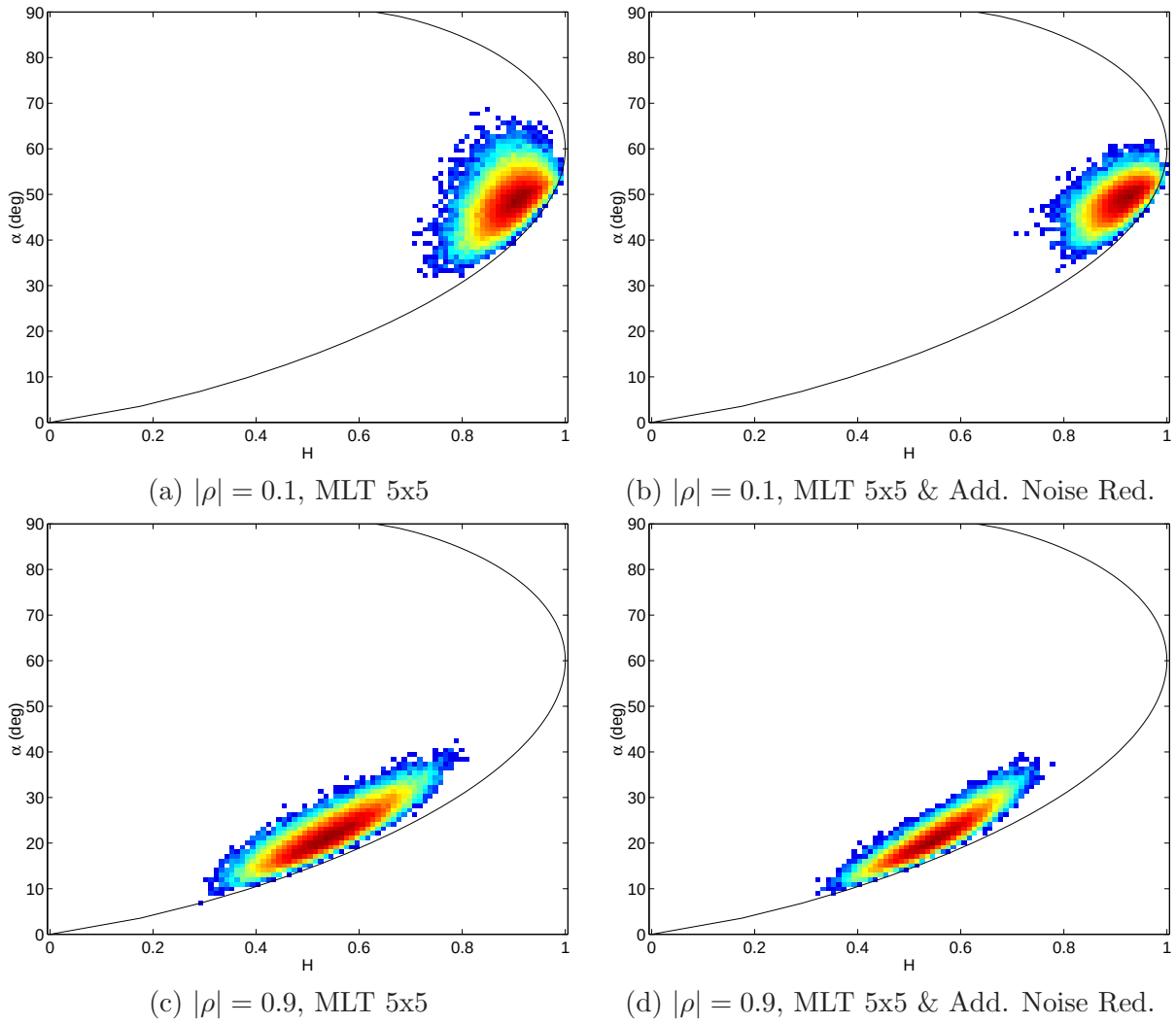

(a) $|\rho| = 0.1$, MLT 5x5

(b) $|\rho| = 0.1$, MLT 5x5 & Add. Noise Red.

(c) $|\rho| = 0.9$, MLT 5x5

(d) $|\rho| = 0.9$, MLT 5x5 & Add. Noise Red.

Figure 7.19: $H/\overline{\alpha}$ maps for simulated data with coherence values $|\rho| = 0.1$ and $|\rho| = 0.9$. Data processed with a standard 5 by 5 multilook, with and without additive speckle noise reduction.

respect to a standard multilook approach, for the same number of averaged pixels.

The second set of polarimetric descriptors which have been analyzed make reference to the covariance matrix $[C]$ considered as a unit, and not as a collection of values. The quantities which have been measured are the entropy H and $\overline{\alpha}$, as defined in Eqs. (7.28) and (7.29) respectively. Figs. 7.18a and 7.18b show these two values for the whole coherence range, for data processed with a 5 by 5 pixel standard multilook and with the proposed algorithm.

Figs. 7.18a and 7.18b prove that to filter the covariance matrix entries differently, but according to the noise mode presented at Chapter 5, does not alter polarimetric information at all. If the entropy H and $\overline{\alpha}$ values derived from data processed with the multilook approach and with the proposed algorithm are compared with theoretical values (dashed line), it can be observed that the values derived in the second case present lower biases. This is a clear consequence of the larger noise reduction induced by the proposed algorithm. This bias reduction is more evident in the case of the entropy H. Fig. 7.19 presents the $H/\overline{\alpha}$ maps obtained with the standard multilook approach with and without additive speckle noise reduction, for two extreme values of coherence. On these maps, one can clearly notice that those derived with the proposed algorithm are characterized by a lower dispersion around the mean values of entropy H and $\overline{\alpha}$, due to the larger noise reduction.

The multidimensional speckle noise reduction algorithm presented in Section 7.4.3 presents two key steps. A first step focused on the correlation's structure estimation and a second one designed to reduce

	$\sigma_{\Re\{S_{hh}S_{hv}^*\}}$	$\sigma_{\Im\{S_{hh}S_{hv}^*\}}$	$\sigma_{\Re\{S_{hh}S_{vv}^*\}}$	$\sigma_{\Im\{S_{hh}S_{vv}^*\}}$	$\sigma_{\Re\{S_{hv}S_{vv}^*\}}$	$\sigma_{\Im\{S_{hv}S_{vv}^*\}}$
MLT 5x5	0.441	0.456	0.834	0.571	0.442	0.459
MLT & ANR	0.307	0.328	0.706	0.404	0.311	0.331
LMMSE	0.414	0.430	0.880	0.536	0.415	0.431
LMMSE & ANR	0.287	0.303	0.777	0.377	0.290	0.303

(a)

	$\lvert\rho\rvert_{S_{hh}S_{hv}^*}$	$\lvert\rho\rvert_{S_{hh}S_{vv}^*}$	$\lvert\rho\rvert_{S_{hv}S_{vv}^*}$
MLT 5x5	0.177	0.608	0.179
MLT 5x5 & ANR	0.123	0.608	0.125
LMMSE	0.167	0.602	0.169
LMMSE & ANR	0.115	0.604	0.117

(b)

	H	σ_H	$\overline{\alpha}$	σ_α
MLT 5x5	0.755	0.066	0.581	0.081
MLT 5x5 & ANR	0.767	0.055	0.571	0.068
LMMSE	0.763	0.066	0.585	0.082
LMMSE & ANR	0.773	0.057	0.573	0.070

(c)

Table 7.3: Results on PolSAR speckle noise reduction. The data's correlation structure is calculated with a 5 by 5 pixel multilook in all the cases. The labels are: MLT for a standard multilook filter, MLT & ANR for the standard multilook with additive speckle noise reduction, LMMSE for the standard multiplicative speckle noise LMMSE filter [1] and LMMSE & ANR for the same LMMSE filter but with additive speckle noise reduction. The theoretical entropy equals $H = 0.789$, whereas $\overline{\alpha} = 0.524$.

	$\sigma_{\Re\{S_{hh}S_{hv}^*\}}$	$\sigma_{\Im\{S_{hh}S_{hv}^*\}}$	$\sigma_{\Re\{S_{hh}S_{vv}^*\}}$	$\sigma_{\Im\{S_{hh}S_{vv}^*\}}$	$\sigma_{\Re\{S_{hv}S_{vv}^*\}}$	$\sigma_{\Im\{S_{hv}S_{vv}^*\}}$
MLT 5x5	0.440	0.457	0.835	0.571	0.441	0.459
MLT & ANR	0.277	0.296	0.754	0.476	0.287	0.299
LMMSE	0.414	0.431	0.880	0.537	0.414	0.431
LMMSE & ANR	0.259	0.276	0.803	0.451	0.269	0.281

(a)

	$\lvert\rho\rvert_{S_{hh}S_{hv}^*}$	$\lvert\rho\rvert_{S_{hh}S_{vv}^*}$	$\lvert\rho\rvert_{S_{hv}S_{vv}^*}$
MLT 5x5	0.177	0.608	0.179
MLT 5x5 & ANR	0.112	0.624	0.115
LMMSE	0.167	0.602	0.168
LMMSE & ANR	0.105	0.620	0.108

(b)

	H	σ_H	$\overline{\alpha}$	σ_α
MLT 5x5	0.756	0.066	0.582	0.082
MLT 5x5 & ANR	0.759	0.061	0.562	0.075
LMMSE	0.764	0.066	0.585	0.082
LMMSE & ANR	0.764	0.062	0.564	0.075

(c)

Table 7.4: Results on PolSAR speckle noise reduction. The data's correlation structure is calculated by the WCCE algorithm with a 40 coefficient Daubechies filter for a 3 scale DWT and $th_w = -1$. The labels are: MLT for a standard multilook filter, MLT & ANR for the standard multilook with additive speckle noise reduction, LMMSE for the standard multiplicative speckle noise LMMSE filter [1] and LMMSE & ANR for the same LMMSE filter but with additive speckle noise reduction. The theoretical entropy equals $H = 0.789$, whereas $\overline{\alpha} = 0.524$.

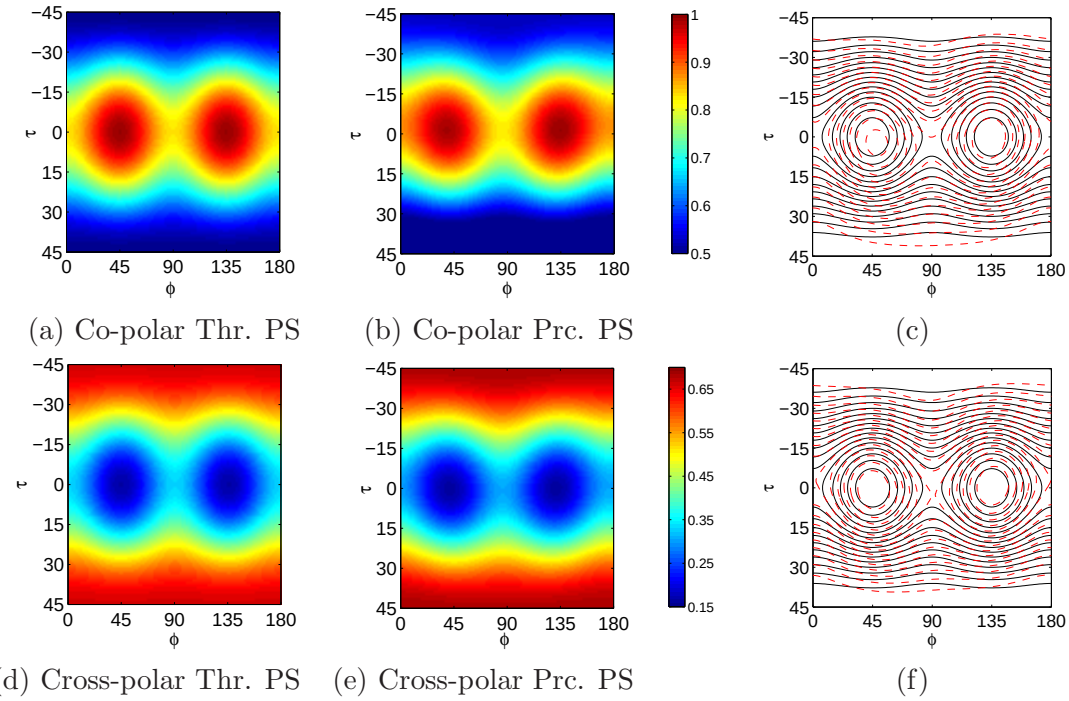

(a) Co-polar Thr. PS (b) Co-polar Prc. PS (c)

(d) Cross-polar Thr. PS (e) Cross-polar Prc. PS (f)

Figure 7.20: Co-polar and cross-polar Polarimetric Signatures (PS). Thr. refers to the theoretical PS whereas Prc. makes reference to the PS derived from processed data. The correlation structure is estimated with the WCCE algorithm and the LMMSE filter is employed to eliminate the multiplicative speckle term.

the multiplicative speckle noise term. In the previous tests, these have been performed by a multilook process. This option, hence, leads to a loss in spatial resolution. On the contrary, when spatial resolution is of interest, a different approach has to be considered. As proposed, a possible alternative is to estimate the data's correlation structure with the WCCE algorithm, see Section 7.3 for details, and to reduce the multiplicative speckle noise component with the LMMSE filter, as presented in [1]. In the following, this new approach is compared with the alternative employed previously based only on multilook filter. In this case, simulated data correspond to a dataset characterized by the covariance matrix given in Eq. (7.31), where $|\rho| = 0.6$ and $\phi_x = 0$ rad. It is important to notice that, in this case, the additive speckle term is the dominant noise component for all the off-diagonal covariance matrix entries. The quantitative results obtained in this case can be observed in Tables 7.3 and 7.4.

A general overview of the results presented in Tables 7.3 and 7.4 prove that the algorithm proposed in Section 7.4.3, leads to a larger noise reduction than standard techniques, as for instance the multilook or the LMMSE filters, without corrupting polarimetric information. This is independent of the procedures employed to estimate the correlation structure and the filter reducing the multiplicative speckle term. Tables 7.3a and 7.4a measure the noise reduction capability in terms of standard deviation (σ). As it can be observed, a larger noise reduction is obtained if the additive speckle noise term is eliminated according to coherence values. This reduction, as concluded from the coherence values presented in Tables 7.3b and 7.4b, and the $H/\overline{\alpha}$ values given by Tables 7.3c and 7.4c does not introduce a bias in the polarimetric information. In the case of the $H/\overline{\alpha}$ values, a small bias is observed since, as shown previously, noise is not completely reduced.

The last point which has been analyzed with simulated data is the maintenance of the PS in the case of a distributed scatterer. The theoretical PS has been compared with the one derived from data processed with the proposed PolSAR filter in which, coherence information is estimated with the WCCE algorithm and the multiplicative speckle noise term is reduced with the LMMSE filter [1]. The results are presented in Fig. 7.20, where it can be noticed that the PS corresponding to the processed data presents a perfect match with the theoretical PS.

7.5.2 Polarimetric Speckle Noise Reduction: Real PolSAR Data

Within this last section, the multidimensional speckle noise filter presented in Section 7.4.3 is tested over a real PolSAR dataset. The data which has been employed correspond to the fully polarimetric dataset, presented in Section 7.3.2, corresponding the area of Oberpfaffenhofen (Germany). In this case, the data's correlation structure will be calculated by means of the WCCE algorithm, in which the 40 coefficient Daubechies wavelet filter is employed to calculate the DWT. The multiplicative speckle term is reduced by means of the LMMSE filter as presented in [1]. The use of these two algorithms make possible to maintain spatial resolution.

Since the diagonal elements of the covariance matrix present a fully multiplicative noise model, the LMMSE filter, as given in [1], with and without additive speckle noise reduction will produce the same results. The differences are produced within the off-diagonal elements, since they contain an additive speckle noise component, whose importance is determined by the complex correlation coefficient. Hence, the improvement due to the reduction of the additive speckle noise term is analyzed by comparing the results corresponding to the LMMSE filter with those where the additive speckle noise term is also reduced. The filtering properties of the proposed multidimensional SAR filter, as well as the capability to preserve the polarimetric information, despite the off-diagonal covariance matrix entries are differently processed, is analyzed in the following.

The first polarimetric quantities to consider are the polarimetric coherences of each one of the covariance matrix elements. The two coherences which are considered correspond to the terms $S_{hh}S_{vv}^*$ and $S_{hh}S_{hv}^*$. The one corresponding to the term $S_{hv}S_{vv}^*$ is not considered since it presents basically the same properties of the coherence corresponding to $S_{hh}S_{hv}^*$. Figs. 7.21a and 7.21b present the histograms of these coherences for the LMMSE filter, with and without additive noise reduction. As it can be observed, the coherences corresponding to the proposed filter are clearly lower than the ones corresponding to the standard LMMSE filter. It can be affirmed, considering the results derived with simulated data, that this bias is originated by the higher noise content if the additive speckle term is not considered. Hence, it can be concluded that the reduction of the additive speckle noise term leads to lower coherence biases.

The entropy H, $\overline{\alpha}$ and the anisotropy A are perfect indicators to analyze the maintenance of the polarimetric properties. Hence, these values are analyzed, as in the case of the coherence values, for the LMMSE filter, with and without additive speckle noise reduction. Figs. 7.22a, 7.22b and 7.22c depict the histograms of these three quantities, whereas the corresponding images are given by Fig. 7.23. A bias between the values corresponding to data derived by means of the standard LMMSE filter with and

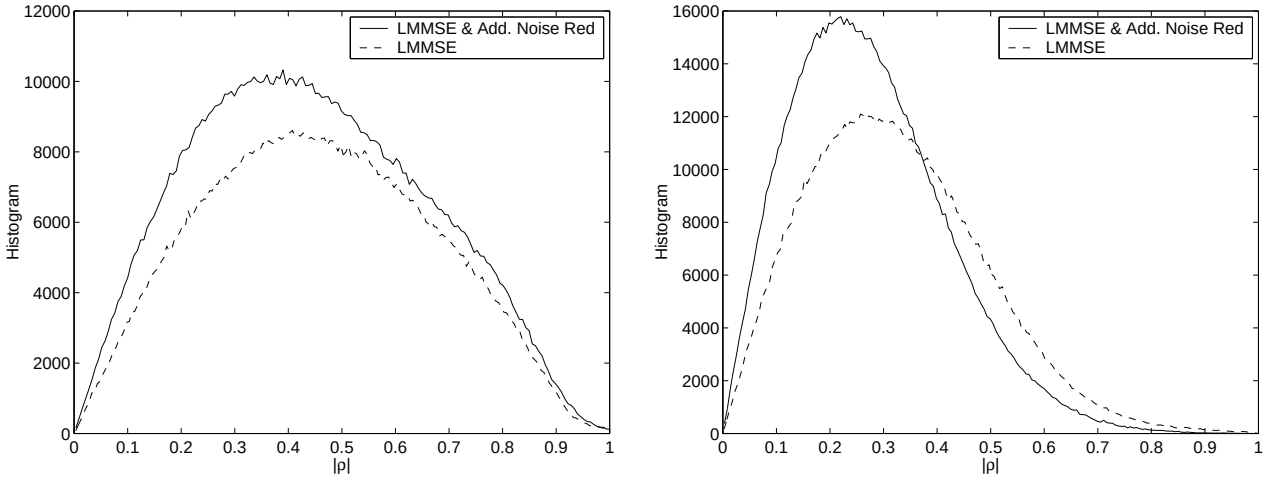

(a)$|\rho_{hhvv}|$ (b) $|\rho_{hhhv}|$

Figure 7.21: Histograms corresponding to the covariance matrix term $S_{hh}S_{vv}^*$ where data have been processed with the standard LMMSE filter with and without the reduction of the additive speckle term.

without the additive noise reduction can be noticed, specially for the anisotropy. As concluded before, the bias observed in the case of the LMMSE filter, in its standard configuration, is due to the higher noise content of data. As it can be observed in the images presented by Fig. 7.23, the polarimetric information is not biased as a consequence of the different amount of filtering applied to the off-diagonal elements of the covariance matrix. On the contrary, the higher speckle noise reduction, specially in those areas with low coherence, leads to a reduction of the biases of the different polarimetric descriptors as a consequence of noise.

The use of the WCCE algorithm to calculate the data's correlation structure and the LMMSE algorithm to eliminate the multiplicative speckle term allows also to maintain the spatial properties of the processed signal. Figs. 7.24 and 7.26 present the results derived for the real and imaginary parts of the covariance matrix terms $S_{hh}S_{vv}^{*}$ and $S_{hh}S_{hv}^{*}$ respectively, whereas Figs. 7.25 and 7.27 show the image details marked with red squares in Figs. 7.2 and 7.6 respectively, whose corresponding original images are given by Figs. 7.12 and 7.13. From these images, it can be observed that the reduction of the additive speckle noise term leads to a larger noise reduction in the final images. As shown, this higher noise reduction does not produces a loss on spatial resolution or spatial details with respect to the original images.

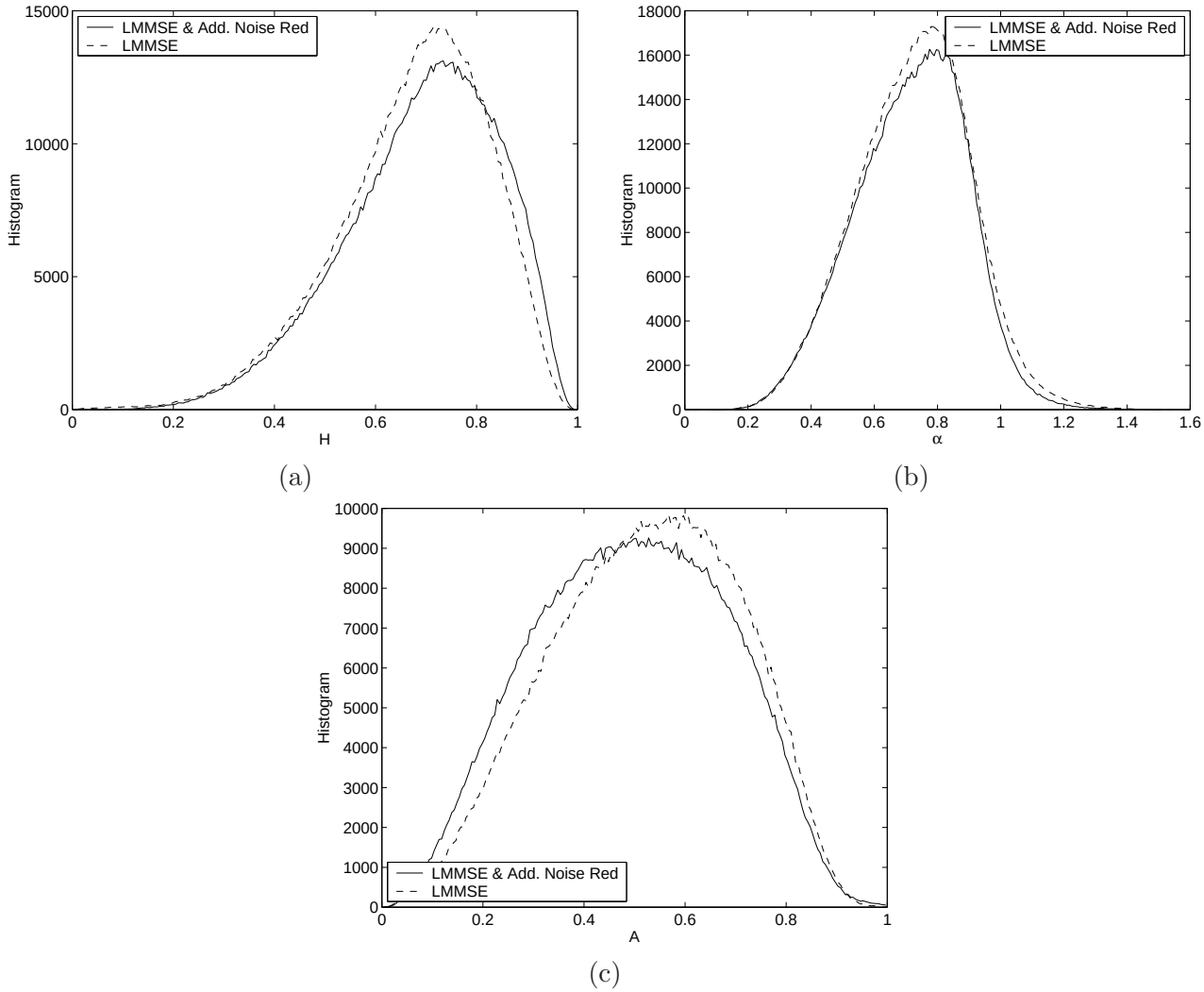

Figure 7.22: Histograms corresponding to the entropy H, $\overline{\alpha}$ and anisotropy A for the Oberpfaffenhofen test site.

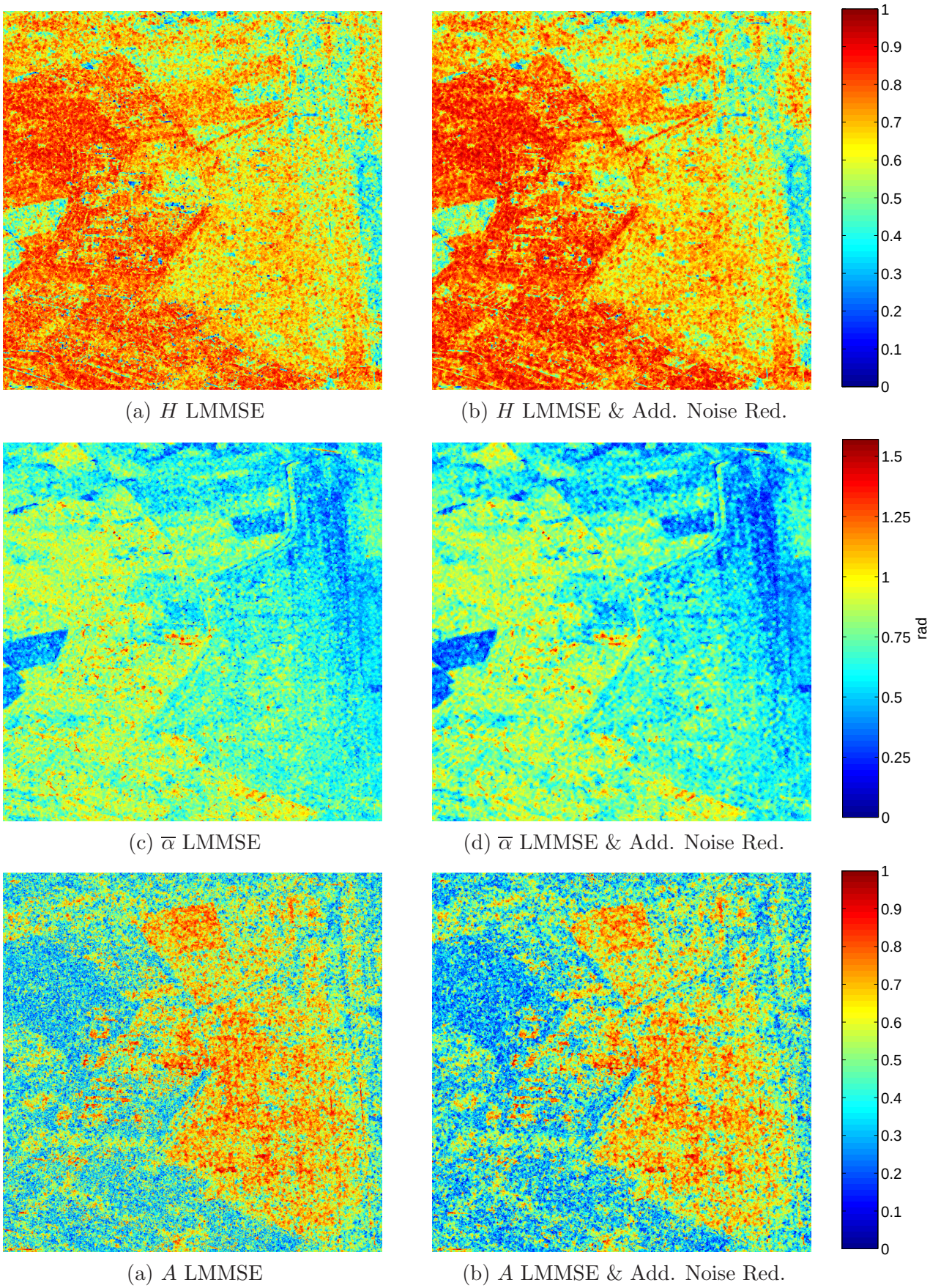

(a) H LMMSE (b) H LMMSE & Add. Noise Red.

(c) $\overline{\alpha}$ LMMSE (d) $\overline{\alpha}$ LMMSE & Add. Noise Red.

(a) A LMMSE (b) A LMMSE & Add. Noise Red.

Figure 7.23: Entropy H, α and Anisotropy A maps for the Oberpfaffenhofen test site.

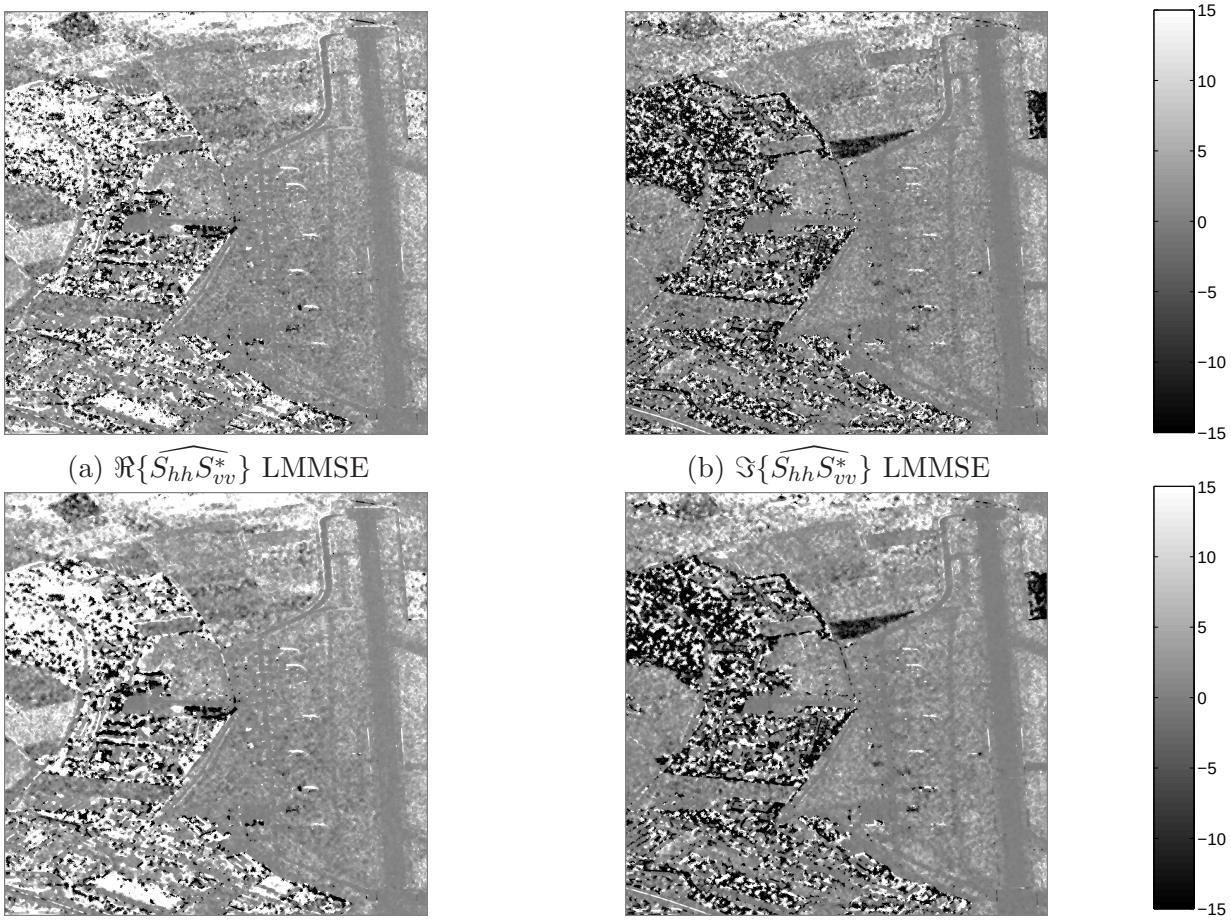

(a) $\Re\{\widehat{S_{hh}S_{vv}^*}\}$ LMMSE (b) $\Im\{\widehat{S_{hh}S_{vv}^*}\}$ LMMSE

(c) $\Re\{\widehat{S_{hh}S_{vv}^*}\}$ LMMSE & Add. Noise Red. (d) $\Im\{\widehat{S_{hh}S_{vv}^*}\}$ LMMSE & Add. Noise Red.

Figure 7.24: Filtered $S_{hh}S_{vv}^*$ covariance matrix term using the LMMSE filter with and without additive speckle noise reduction.

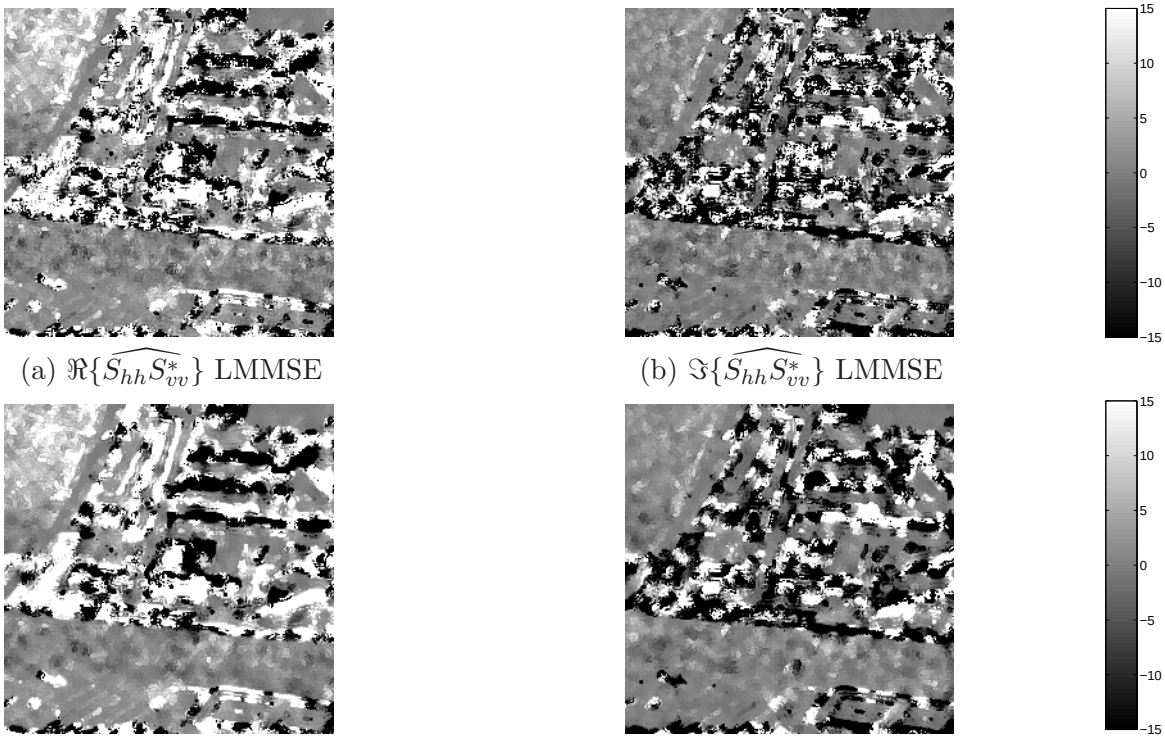

(a) $\Re\{\widehat{S_{hh}S_{vv}^*}\}$ LMMSE (b) $\Im\{\widehat{S_{hh}S_{vv}^*}\}$ LMMSE

(c) $\Re\{\widehat{S_{hh}S_{vv}^*}\}$ LMMSE & Add. Noise Red. (d) $\Re\{\widehat{S_{hh}S_{vv}^*}\}$ LMMSE & Add. Noise Red.

Figure 7.25: Detail images of the filtered $S_{hh}S_{vv}^*$ covariance matrix term using the LMMSE filter with and without additive speckle noise reduction.

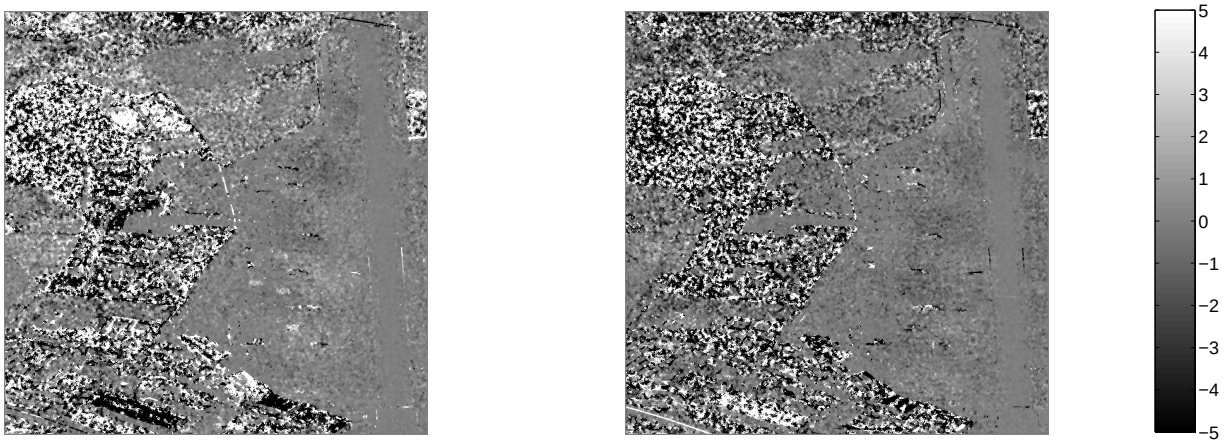

(a) $\Re\{\widehat{S_{hh}S_{hv}^*}\}$ LMMSE (b) $\Im\{\widehat{S_{hh}S_{hv}^*}\}$ LMMSE

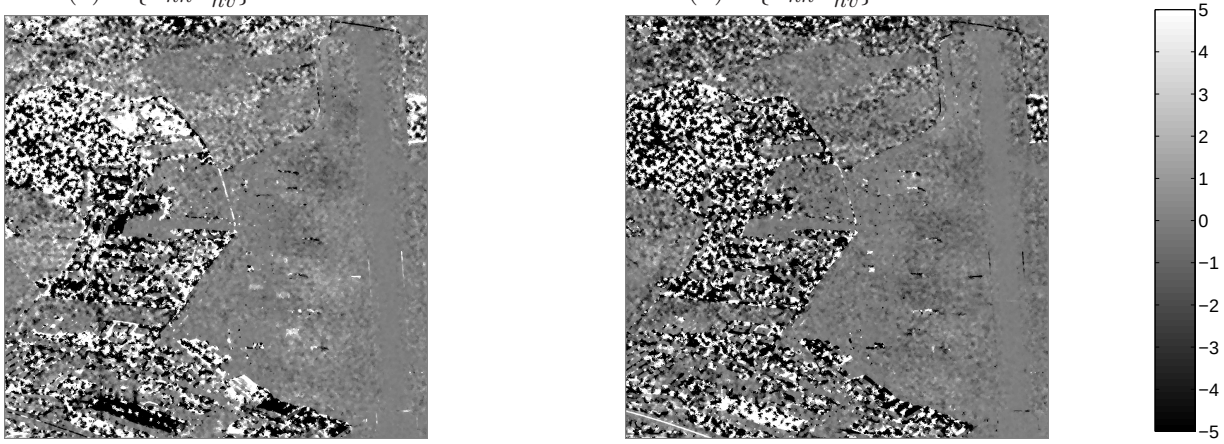

(c) $\Re\{\widehat{S_{hh}S_{hv}^*}\}$ LMMSE & Add. Noise Red. (d) $\Im\{\widehat{S_{hh}S_{hv}^*}\}$ LMMSE & Add. Noise Red.

Figure 7.26: Filtered $S_{hh}S_{hv}^*$ covariance matrix term using the LMMSE filter with and without additive speckle noise reduction.

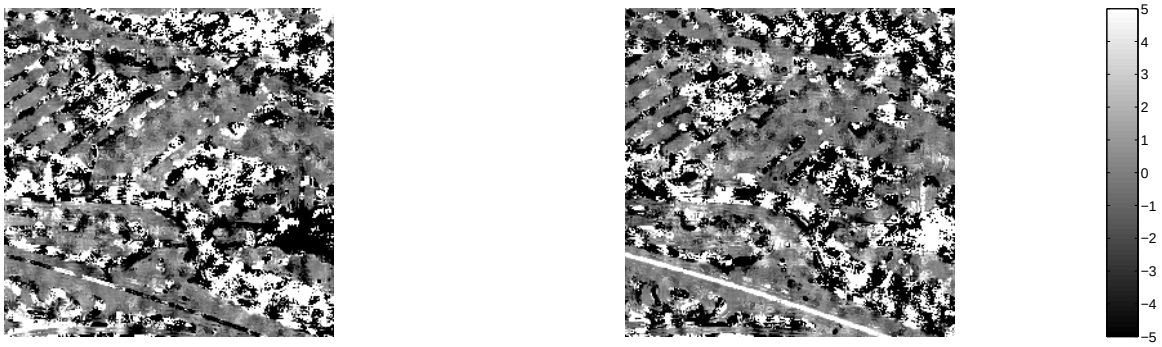

(a) $\Re\{\widehat{S_{hh}S_{hv}^*}\}$ LMMSE (b) $\Im\{\widehat{S_{hh}S_{hv}^*}\}$ LMMSE

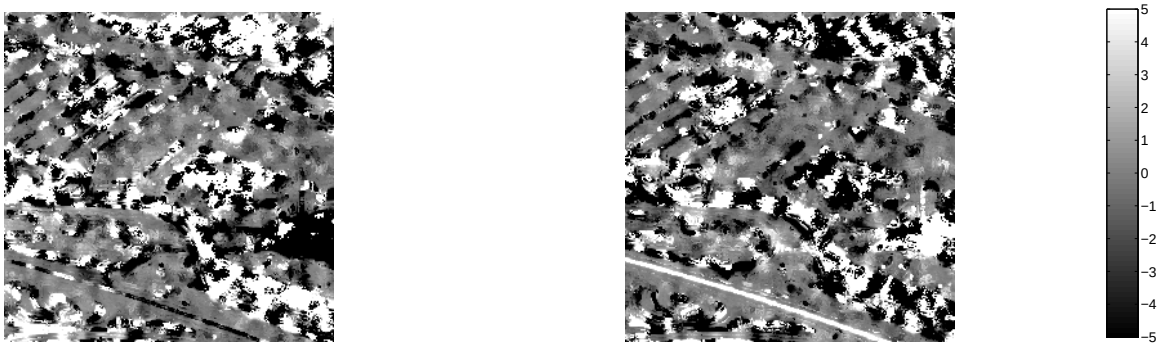

(c) $\Re\{\widehat{S_{hh}S_{hv}^*}\}$ LMMSE & Add. Noise Red. (d) $\Re\{\widehat{S_{hh}S_{hv}^*}\}$ LMMSE & Add. Noise Red.

Figure 7.27: Detail images of the filtered $S_{hh}S_{hv}^*$ covariance matrix term using the LMMSE filter with and without additive speckle noise reduction.

7.6 Multidimensional SAR Data Speckle Filtering: Principles

This section collects, on the one hand, the implications of the multidimensional speckle noise model presented at Chapter 5, and, on the other hand, the results which have been presented throughout all this chapter, with the objective to define new principles concerning multidimensional SAR speckle noise filtering.

As demonstrated and validated in Chapter 5, the speckle's noise nature for multidimensional SAR data depends on the data's correlation structure. For this data expressed under a covariance matrix formulation, it was proved that for a particular complex Hermitian product of SAR images, the speckle noise, for the real and imaginary parts, is characterized by an additive nature for low coherences. In those cases in which the real or the imaginary parts of the complex correlation coefficient are close to one, they produce speckle noise to be characterized in these cases by a multiplicative behavior. Therefore, in order to reduce noise speckle optimally, it is necessary to perform this noise reduction according to the data's correlation structure. This usage of correlation information, i.e., coherence, is headed for an optimal noise reduction for every covariance matrix element and is not employed to find and optimal combination of these elements to maximize noise reduction. As a result, polarimetric information is preserved.

Since the elements of the covariance matrix are characterized by presenting different coherence values, the amount of multiplicative and additive speckle noises, varies form entry to entry. Hence, this fact produces that the optimum filtering differs for the different covariance matrix entries. As it has been demonstrated in this chapter, to process the elements differently, does not represent a loss of polarimetric properties, unless the filtering is not performed according to the speckle noise model presented in Chapter 5. On the contrary, to process differently the elements of the covariance matrix, but according to the correct multidimensional speckle noise model, leads to an improvement on the estimation of the different polarimetric indicators, and to a larger noise reduction.

The previous paragraphs allow to establish new principles for multidimensional SAR speckle filtering, and for PolSAR speckle filtering in particular. These principles are:

- Speckle noise has to be reduced over second order moments data descriptors. The best choice for this is the covariance matrix $[C]$, since all his entries are constructed as Hermitian products. This allows to make use of the speckle noise model, which is the same for all the elements.
- For every covariance matrix element, speckle presents a behavior depending on the complex correlation coefficient characterizing it. Hence, this coefficient must be estimated in order to optimize speckle noise reduction.
- The elements of the covariance matrix have to be processed according to their particular complex correlation coefficient in accordance with the proposed speckle noise model. This produces an optimum noise reduction.
- In order to maintain the spatial resolution and the image details both, the estimation of the data's correlation structure, as well as the reduction of the multiplicative noise component, have to performed with algorithms preserving it.

7.7 Summary

This chapter represents a synthesis of the three previous chapters of this thesis. The main idea behind this chapter is the reduction of speckle noise effects in multidimensional SAR imagery, with special attention to polarimetric SAR data. The availability of the multidimensional speckle noise model, obtained in Chapter 5, has made possible to define an optimum multidimensional speckle noise filter. This filter is based on novel speckle noise reduction principles, which are derived precisely, as a result of the multidimensional speckle noise model.

Within the first part of this chapter, it is demonstrated that the algorithm defined in Chapter 6 to estimate the complex correlation coefficient can be extended to estimate it in the case of a general Hermitian product, with a high spatial resolution. The main result of this extension is that it is possible to estimate the multidimensional SAR data's correlation structure, with a high spatial precision, by applying the algorithm to each one of the covariance matrix entries. In some cases, this is the only desired information from multidimensional SAR data. The performance and validity of this approach to calculate the correlation structure is specifically tested with polarimetric SAR data.

The previous approach is not sufficient to estimate the full covariance matrix. To perform this task, and on the basis of the Hermitian product speckle noise model presented in Chapter 5, the Hermitian product linear minimum square error estimator (LMMSE) is derived. Due to the complexity of this novel noise model, some approximations have to be introduced in the derivation. Despite the approximations make the use of the LMMSE approach unpractical, the derived expression permits to extract two important conclusions concerning the optimum filtering of the Hermitian product. On the one hand, the optimum filtering has to be performed according to the complex correlation coefficient. On the other hand, to consider a multiplicative noise model only leads to signal underfiltering.

In the last part of this chapter, the ideas behind the LMMSE approach are considered to define a new multidimensional speckle noise filter, with special attention to polarimetric SAR data. This algorithm works in a two step process. In the first step, the covariance matrix additive speckle noise component is reduced on the basis of the data's correlation structure, whereas the multiplicative speckle noise component is reduced in a second step by means of standard techniques. The most important feature of this algorithm is that it process the covariance matrix entries differently. As demonstrated, this does not lead to a destruction of the properties of the signal. In the case polarimetric SAR data, it is proved that the average scattering mechanism is fully preserved. Indeed, the larger noise reduction, consequence of considering the additive speckle term, leads to a reduction of the biases of the different polarimetric quantities as entropy or anisotropy. As it has been presented in the last part of the chapter, it is possible to estimate the covariance matrix maintaining all its properties and the spatial resolution of the data, if the proposed multidimensional speckle filter considers techniques specially designed to the analysis of high spatial resolution signals.

As it has been shown in this chapter, the availability of the multidimensional SAR data speckle noise model makes possible to extend the properties of multidimensional speckle noise filters. As a consequence, the last part of this chapter contains new principles concerning the definition of an optimum multidimensional speckle noise filter.